Title

Hippocampus and amygdala fear memory engrams re-emerge after contextual fear reinstatement

Authors

Yosif Zaki[1,3], William Mau[1,3], Christine Cincotta[2], Anahita Hamidi[2], Emily Doucette[2], Stephanie L. Grella[2], Emily Merfeld[2], Nathen J. Murawski[2], Monika Shpokayte[2], Steve Ramirez[2,4,*].

[1]Department of Neuroscience, School of Medicine at Mount Sinai, New York, NY, 10029
[2]Department of Psychological and Brain Sciences, Boston University, Boston, MA, 02215
[3]These authors contributed equally to this work
[4]Lead Contact
[*]Correspondence: dvsteve@bu.edu

Abstract

The formation and extinction of fear memories represent two forms of learning that each engage the hippocampus and amygdala. How cell populations in these areas contribute to fear relapse, however, remains unclear. Here, we demonstrate that, in mice, cells active during fear conditioning in the dentate gyrus of hippocampus and basolateral amygdala exhibit decreased activity during extinction and are re-engaged after fear reinstatement. *In vivo* calcium imaging reveals that reinstatement drives population dynamics in the basolateral amygdala to revert to a network state similar to the state present during fear conditioning. Finally, we find that optogenetic inactivation of neuronal ensembles active during fear conditioning in either the hippocampus or amygdala is sufficient to disrupt fear expression after reinstatement. These results suggest that fear reinstatement triggers a partial re-emergence of the original fear memory representation, providing new insight into the neural substrates of fear relapse.

Introduction

The biological capacity to produce adaptive behavioral responses in actively changing environments is critical to an animal's survival. Contextual fear conditioning (CFC) is a form of learning whereby an animal learns to associate a conditioned stimulus (e.g. a context) with an unconditioned aversive stimulus (e.g. foot shocks) to produce a conditioned response to the conditioned stimulus (e.g. freezing). Conditioned responses can be mitigated through extinction learning via repeated exposure to the conditioned context in the absence of the foot shock. However, while extinction learning can be effective at attenuating fear, animals are susceptible to fear relapse under several conditions, including exposure to stressors, the passage of time, and re-exposure to the unconditioned stimulus (Goode, Jin, & Maren, 2018). This observation in rodents shares numerous similarities to clinical observations: exposure therapy – a clinical analog to extinction learning – can be effective at reducing fear in subsets of patients with anxiety disorders or post-traumatic stress disorder. However, many patients are still susceptible to fear relapse following successful exposure therapy (Kearns, Ressler, Zatzick, & Rothbaum, 2012). Despite an extensive body of literature investigating the neural substrates of fear and extinction learning (Maren, 2001), how discrete neuronal populations causally contribute to fear relapse remains incompletely understood.

Previous studies have demonstrated that cells in the dorsal dentate gyrus of the hippocampus (DG) and in the basolateral amygdala (BLA) that are active during fear conditioning (hereafter referred to as the DG and BLA fear ensembles) are preferentially re-

activated during fear memory recall (Ramirez et al., 2013; Reijmers, Perkins, Matsuo, & Mayford, 2007), and are necessary and sufficient for the expression of defensive behaviors such as freezing (Denny et al., 2014; Redondo et al., 2014). Additionally, recent evidence has indicated that extinction learning may be mediated by interactions between local BLA interneurons and a BLA fear ensemble (Davis, Zaki, Maguire, & Reijmers, 2017), while a new set of cells simultaneously emerges in both the hippocampus (Khalaf et al., 2018; Lacagnina et al., 2019; Tronson et al., 2009) and BLA (Herry et al., 2008), possibly to encode extinction learning. However, whether fear relapse re-engages the original memory-encoding neuronal population or gives rise to a new representation remains unclear.

Results

To address this, we first developed a behavioral protocol for fear reinstatement, a model of fear relapse in rodents (Rescorla & Heth, 1975). Mice underwent CFC and two subsequent extinction (EXT) sessions over two days, followed by an immediate shock (IS) in a novel context to reinstate the original fear memory, and a post-reinstatement recall test (IS-Recall) the following day to measure the return of fear (Figure 1a, bottom behavioral schedule). Reinstatement led to an increase in freezing in the original conditioned context (Figure 1—figure supplement 1a-e) and was largely context specific (Figure 1—figure supplement 2a,b).

Next, we determined if the cells active during fear conditioning were preferentially re-activated after mice underwent extinction and subsequent reinstatement. To that end, we tagged cells active during fear conditioning by injecting an activity-dependent viral cocktail of AAV9-c-Fos-tTA and AAV9-TRE-eYFP in the DG and BLA of adult male mice (Figure 1b,c). This virus enabled expression of eYFP in cells sufficiently active to express the immediate early gene c-Fos, which is under the repressive control of the antibiotic doxycycline (DOX)(Reijmers et al., 2007). We then measured immunoreactive c-Fos and calculated overlap between the set of cells active during CFC (eYFP-expressing cells) and during different stages of the behavioral schedule (c-Fos-expressing cells) (Figure 1d,e).

Previous reports have shown that the number of BLA cells active during both fear conditioning and fear memory recall correlates with freezing levels (Reijmers et al., 2007). Thus, we reasoned that if reinstatement re-engages the fear ensemble, the set of cells active during fear conditioning would be active again following reinstatement, and freezing during recall would correlate with cellular overlap. We found that, as expected, cells active during CFC were highly re-activated during Recall the following day, and EXT led to a modest, non-significant decrease in overlap. Interestingly, compared to EXT-Recall, mice exhibited more overlap in the BLA after reinstatement during a post-reinstatement recall session (IS-Recall) (Figure 1f). However, freezing behavior during Recall sessions did not correlate with BLA fear ensemble re-activation across the FC-Recall, EXT-Recall, and IS-Recall groups, indicating that BLA fear ensemble activity may not be predictive of freezing across these behavioral conditions (Figure 1g). The IS-Recall group exhibited greater overall expression of cFos than the EXT-Recall group, but less overall expression of eYFP than the EXT-Recall group; overall expression of cFos and eYFP was otherwise stable across groups (Figure 1—figure supplement 1f,g).

In the DG, we similarly observed significant overlap between the set of cells active during CFC and cells active during fear memory recall, as previously reported (Ramirez et al., 2013) (Figure 1h). In support of the notion that the dorsal DG processes changes in environmental contingencies (Fanselow & Dong, 2010), this overlap substantially decreased after EXT. While overlap remained low after IS, it significantly increased when mice were given

the IS and were placed back into the original conditioned context the following day, suggesting that fear reinstatement may re-engage the set of cells originally active during fear conditioning (Figure 1h). Additionally, unlike BLA overlaps, freezing behavior correlated with overlaps in the DG across all groups (Figure 1i), indicating that DG fear ensemble re-activation was predictive of freezing. Overall expression of eYFP and cFos was stable across groups in DG (Figure 1—figure supplement 1h,i).

Whereas our c-Fos-based labeling system allowed comparisons between activity of cells across two discrete timepoints with high spatial resolution, it was incapable of measuring activity at finer timescales due to the slow kinetics of immediate-early gene expression relative to real-time neural activity. To overcome this weakness, we next utilized an *in vivo* calcium (Ca^{2+}) imaging approach to record real-time neuronal activity in the BLA in freely moving mice during exposures to both a conditioned context and a neutral context where no shocks were delivered (Figure 2a-b). We tracked these cells longitudinally over the course of the reinstatement schedule, in order to determine whether shared population dynamics are associated with both fear conditioning and reinstatement (Sheintuch et al., 2017) (Figure 2c; see also Figure 2—figure supplement 2). To define initial population states, we constructed Ca^{2+} transient rate population vectors from the CFC session for each mouse. Then, to compare extinction and post-reinstatement recall states to CFC, we correlated population vectors from EXT and Recall (in 30 s non-overlapping time windows) to the CFC population vector. We found that over EXT, the population states in the BLA gradually deviated from its state during CFC, supporting the idea of a network-wide transformation over extinction (Grewe et al., 2017; Hartley et al., 2019; Herry et al., 2008; Tronson et al., 2009) (Figure 2d). However, during Recall, the BLA population rebounded towards the CFC network state to an extent greater than expected by chance (Figure 2e, left). These effects were absent in a neutral context and in CA1 of hippocampus (Figure 2e, right; see also Figure 2—figure supplement 1), demonstrating that the conditioned context and BLA drove these dynamics. Next, using an algorithm for extracting co-active neurons from simultaneously recorded cells (Lopes-dos-Santos, Ribeiro, & Tort, 2013), we characterized neuronal ensembles that were highly active during individual sessions (CFC, EXT1, and EXT2). Then, during Recall, we correlated the activity of these ensembles to freezing and found that the activity of ensembles extracted during CFC and EXT1 reliably predicted relapse freezing, but the ensembles extracted during EXT2 did not (Figure 2f). No ensembles predicted freezing in the neutral context. This suggested that BLA activity patterns contributed to expression of fear relapse, but only before extinction training modified these patterns. Overall, these data indicated that context-specific reinstated fear was associated with the emergence of network states in the BLA that resembled network states during fear conditioning, suggesting that a relapsed fear memory may be represented by a similar trace as the original fear memory.

Finally, we sought to determine whether the activity of cells active during fear conditioning was necessary for expression of reinstated fear. To do this, we bilaterally injected mice in either the DG or the BLA with a virus cocktail of AAV9-c-Fos-tTA and AAV9-TRE-ArchT-eYFP to drive expression of the light-sensitive protein archaerhodopsin (ArchT) in cells active during CFC, and subsequently implanted optic fibers above the injection sites (Figure 3a,b). Mice then underwent two EXT sessions, the reinstating shock, and recall the following day (Figure 3c). Mice in both the DG and BLA experimental groups showed significant suppression of freezing during optical inhibition. This manipulation was reversible, as freezing increased again in the following light-off epoch (Figure 3d,e). eYFP controls did not show this decrease in

138 freezing during optical inhibition, confirming that the behavioral effect was dependent on
139 expression of ArchT (Figure 3f,g).
140 Since the BLA is widely acknowledged as a necessary hub for fear learning (Bocchio,
141 Nabavi, & Capogna, 2017), we next probed whether activity of the BLA fear ensemble during
142 the reinstating shock was necessary or sufficient to induce fear reinstatement. To test necessity,
143 we adopted a similar approach as above in order to express ArchT selectively within the BLA
144 fear ensemble, and then implanted optic fibers bilaterally above BLA (Figure 3—figure
145 supplement 1a,b). Mice underwent FC and EXT, had the BLA fear ensemble inhibited during the
146 reinstating shock, and were then returned to the original conditioned context to assess whether
147 reinstatement could be prevented (Figure 3—figure supplement 1c,d). Surprisingly, mice that
148 had the BLA fear ensemble inhibited did not freeze any less during post-reinstatement recall than
149 eYFP controls (Figure 3—figure supplement 1e). To test sufficiency, we selectively expressed
150 ChR2 in either the BLA fear ensemble or DG fear ensemble in separate groups of mice. Mice
151 underwent FC and EXT, were then placed in a novel chamber, and rather than receiving the
152 reinstating shock, mice had either the BLA or DG fear ensemble stimulated for 60 seconds. The
153 next day, they were placed back in the original conditioned context to assess whether the
154 stimulation could mimic reinstatement (Figure 3—figure supplement 2a-c). Mice that had the
155 BLA fear ensemble stimulated froze no more than eYFP controls (Figure 3—figure supplement
156 2d), while mice that had the DG fear ensemble stimulated only showed modest, non-significant
157 increases in freezing relative to the eYFP controls (Figure 3—figure supplement 2e). These
158 results indicated that despite a crucial role for the BLA and DG fear ensembles in fear learning,
159 activity of these populations was not sufficient to drive fear reinstatement, and activity of the
160 BLA population was not necessary to drive reinstatement either.
161 To test whether the functional role for these cells emerged only after reinstatement or if
162 inhibition of the fear ensemble could suppress freezing during extinction, we inhibited the DG or
163 BLA fear ensemble during an extinction recall session—when low levels of freezing were still
164 present—and observed that inhibition of the DG fear ensemble led to a mild reduction in
165 freezing, while inhibition of the BLA fear ensemble did not disrupt freezing (Figure 3—figure
166 supplement 3). These results suggested that extinction differentially modified the BLA and DG
167 fear ensembles, such that BLA ensemble inhibition did not disrupt freezing during extinction,
168 while DG ensemble activity may have been actively involved in contextual fear expression
169 during extinction.
170 We next determined whether nonspecific manipulation of DG or BLA cells could reduce
171 freezing responses, as opposed to being driven specifically by the fear ensemble in these regions.
172 We tagged cells either in the DG or the BLA that were active during female exposure—an
173 unrelated experience of opposing valence, which has previously been shown to label similar
174 proportions of neurons in both the DG and BLA (Chen et al., 2019; Ramirez et al., 2013;
175 Redondo et al., 2014)—and inhibited those cells during post-reinstatement recall (Figure 3h).
176 Interestingly, whereas this manipulation in the BLA did not cause behavioral changes, inhibition
177 of non-fear cells in the DG led to a modest light-induced reduction in freezing (Figure 3i,j).
178 These results are consistent with the notion that perturbing DG dynamics can produce a general
179 modulation of freezing responses, while only inhibition of BLA fear cells directly disrupts
180 freezing per se. Difference scores between freezing during light-on vs light-off epochs revealed
181 that inhibition of DG fear cells led to moderately less freezing during light-on epochs compared
182 to eYFP controls (Figure 3k), while inhibition of BLA fear cells led to significantly less freezing
183 during light-on epochs (Figure 3l). Finally, one-sample z-tests on difference scores revealed that

184 only mice that had the fear ensemble inhibited (experimental groups; Exp) froze significantly
185 less during light-on epochs than light-off epochs, whereas mice that had female exposure cells
186 inhibited (positive; Pos) and eYFP control mice (eYFP) froze no differently during light-on and
187 light-off epochs (Figure 3m).
188
189 **Discussion**
190 The dynamic nature of fear memory expression constitutes a difficult problem for
191 mitigating fear in the clinic: patients with fear-related disorders who have undergone successful
192 treatment are still prone to relapse, and the underlying causal mechanisms facilitating fear
193 reinstatement are largely unknown. A commonly held view is that fear extinction is not an
194 unlearning of the original trauma; rather, a second memory develops that suppresses the original
195 aversive memory. This raises an important notion about the nature of the ensemble regulating
196 fear expression post-reinstatement. One idea is that the original ensemble driving fear expression
197 and a new ensemble driving fear suppression actively compete to influence behavioral output.
198 Under this framework, fear relapse could be the result of the fear ensemble dominating.
199 Alternatively, fear relapse might be driven by recruitment of a new, discrete cellular population
200 that does not involve the original fear ensemble. A likely scenario is a mixture of the two, where
201 fear relapse materializes from a partial re-emergence of the original ensemble in parallel with
202 recruitment of new neuronal connections (Clem & Schiller, 2016), which our c-Fos labeling,
203 Ca^{2+} imaging, and optogenetics evidence collectively support.
204 Ca^{2+} imaging and c-Fos labeling during the fear reinstatement schedule enabled us to
205 capture network dynamics from the hippocampus and amygdala over multiple timescales,
206 shedding light on the activity of these regions over fear reinstatement. Consistent with prior
207 reports of BLA cell populations up- and down-regulating their activity during extinction learning
208 (Grewe et al., 2017; Herry et al., 2008), and with immediate-early gene data presented here, we
209 observed decorrelation of the BLA population vector from the initial fear-encoding state over
210 repeated exposures to the conditioned context. This time-dependent transformation has
211 previously been depicted in numerous brain regions as "representational drift" (Driscoll, Pettit,
212 Minderer, Chettih, & Harvey, 2017; Mankin et al., 2012; Mau et al., 2018; Rubin, Geva,
213 Sheintuch, & Ziv, 2015; Rule, O'Leary, & Harvey, 2019), but these studies all described
214 population states that monotonically drifted *away* from a reference session. In the present study,
215 the BLA representation exhibited similar dynamics, but in contrast to past work, regressed its
216 neural trajectory *back towards* the initial representation after fear reinstatement. This leads us to
217 believe that fear reinstatement may be restoring a remote memory trace similar to how related
218 optogenetic studies artificially induce memory retrieval (Liu et al., 2012; Ramirez et al., 2013;
219 Redondo et al., 2014).
220 Interestingly, the neural patterns associated with fear expression are still retrievable after
221 putative circuit remodeling over extinction learning and fear reinstatement (Bocchio et al., 2017;
222 Davis et al., 2017; Hartley et al., 2019; Maren, 2015). Our ability to observe and manipulate the
223 original fear ensemble after reinstatement is suggestive of a latent representation of the original
224 memory that persists and coexists with the newly formed extinction memory (Lacagnina et al.,
225 2019; Maren, 2011). However, this new extinction memory may also facilitate local synaptic
226 remodeling that modifies the original fear memory, which may explain why inhibition of the fear
227 ensemble in DG and BLA did not fully eliminate freezing. The re-emergence of the original fear
228 memory may also depend on strict plasticity mechanisms, which can explain why we failed to
229 optically induce relapse through broad stimulation of the BLA fear ensemble after extinction

(Figure 3—figure supplement 2). These results suggest that the natural endogenous fear reinstatement process might require certain activity patterns for modifying the original fear ensemble that could not be artificially produced through BLA stimulation alone. For example, recent work showed that sequential activity from triplets of BLA neurons preceded fear learning (Reitich-Stolero & Paz, 2019) and similar patterns may underlie fear reinstatement. Fear reinstatement may then be recruiting a subset of the original fear ensemble while forming new synaptic linkages with a novel cell population. Others have shown that unique memories reside in patterns of connectivity between memory-encoding – or engram – cells in the hippocampal system (Abdou et al., 2018; Ryan, Roy, Pignatelli, Arons, & Tonegawa, 2015; Tonegawa, Morrissey, & Kitamura, 2018). In the context of our study, reinstatement could be modifying these functional linkages to engage a new set of engram cells, possibly those that are highly excitable at the time of the experience (Cai et al., 2016; Rashid et al., 2016; Yiu et al., 2014), forming a reinstatement ensemble that is similar, but not identical, to the original fear ensemble. In accordance with this idea, post-reinstatement recall activates a large proportion, but not all, of the original fear ensemble (Figure 1f,h).

While our optogenetic experiments suggest a re-emergence of the fear ensemble in the DG, we were unable to perform calcium imaging in DG due to the technical limitations of accessing this region without significant damage to overlying hippocampal subareas. Nonetheless, we report that CA1 exhibits only marginally significant ($p = 0.075$, Figure 2—figure supplement 1b) reversion of calcium dynamics to a fear conditioning-like state after reinstatement. This may be due to the functional differences between DG and CA1, with CA1 possibly responding to more contextual features of the experience (Tanaka et al., 2018) or being overall more subject to plasticity than DG. As others have found, day-to-day dynamics of spatial activity in DG are more stable than in CA1 (Hainmueller & Bartos, 2018). Until methods are developed that allow unfettered imaging of DG while still preserving superficial hippocampal areas, it remains unknown whether the real-time network activity of DG exhibit relapse-induced reactivation of fear ensembles. However, recent work agrees with our prediction that extinction suppresses fear-related activity in the DG while those activity patterns are retrieved during relapse (Lacagnina et al., 2019).

Further work exploring the competing interactions of cellular networks across fear learning and fear suppression could provide important insight into how the brain competes for the expression of fear throughout fear extinction and relapse. Moreover, a deeper understanding of how fear memories are modified by time and experience may help guide development of treatments for trauma-related disorders, and these findings point to hippocampal- and BLA-mediated engrams as key nodes contributing to the re-emergence of a contextual fear memory.

Acknowledgements

We thank Dr. Joshua Sanes and his lab at the Center for Brain Science, Harvard University, for providing laboratory space within which the initial experiments were conducted, the Center for Brain Science Neuroengineering core for providing technical support, and the Society of Fellows at Harvard University for their support. We also thank Dr. Susumu Tonegawa and his lab for providing the activity-dependent virus cocktail, Dr. Chris MacDonald for consultation on behavioral schedules, and Drs. Leon Reijmers and Patrick Davis, for their help with formulating this project and for their feedback throughout. We also thank Vardhan Dani and Inscopix for their technical assistance as well as Helen Fawcett and the NSF Neurophotonics Research Traineeship Program for funding and support. This work was supported by an NIH Early Independence Award (DP5 OD023106-01), an NIH Transformative R01 Award, a Young Investigator Grant from the Brain and Behavior Research Foundation, a Ludwig Family Foundation grant, and the McKnight Foundation Memory and Cognitive Disorders award.

Author Contributions

Y.Z. and S.R. conceived the study. Y.Z., W.M., and S.R. designed experiments and analyzed data. Y.Z., W.M., C.C., A.H., E.D., S.L.G., E.M., N.J.M., and M.S. conducted experiments. Y.Z., W.M., and S.R. wrote the manuscript; all authors edited and commented on the manuscript.

Declaration of Interests

The authors declare no competing interests.

References

Abdou, K., Shehata, M., Choko, K., Nishizono, H., Matsuo, M., Muramatsu, S. I., & Inokuchi, K. (2018). Synapse-specific representation of the identity of overlapping memory engrams. *Science, 360*(6394), 1227-1231. doi:10.1126/science.aat3810

Bocchio, M., Nabavi, S., & Capogna, M. (2017). Synaptic Plasticity, Engrams, and Network Oscillations in Amygdala Circuits for Storage and Retrieval of Emotional Memories. *Neuron, 94*(4), 731-743. doi:10.1016/j.neuron.2017.03.022

Cai, D. J., Aharoni, D., Shuman, T., Shobe, J., Biane, J., Song, W., . . . Silva, A. J. (2016). A shared neural ensemble links distinct contextual memories encoded close in time. *Nature, 534*(7605), 115-118. doi:10.1038/nature17955

Chen, B. K., Murawski, N. J., Cincotta, C., McKissick, O., Finkelstein, A., Hamidi, A. B., . . . Ramirez, S. (2019). Artificially Enhancing and Suppressing Hippocampus-Mediated Memories. *Curr Biol, 29*(11), 1885-1894 e1884. doi:10.1016/j.cub.2019.04.065

Clem, R. L., & Schiller, D. (2016). New Learning and Unlearning: Strangers or Accomplices in Threat Memory Attenuation? *Trends Neurosci, 39*(5), 340-351. doi:10.1016/j.tins.2016.03.003

Davis, P., Zaki, Y., Maguire, J., & Reijmers, L. G. (2017). Cellular and oscillatory substrates of fear extinction learning. *Nat Neurosci, 20*(11), 1624-1633. doi:10.1038/nn.4651

Denny, C. A., Kheirbek, M. A., Alba, E. L., Tanaka, K. F., Brachman, R. A., Laughman, K. B., . . . Hen, R. (2014). Hippocampal memory traces are differentially modulated by experience, time, and adult neurogenesis. *Neuron, 83*(1), 189-201. doi:10.1016/j.neuron.2014.05.018

Driscoll, L. N., Pettit, N. L., Minderer, M., Chettih, S. N., & Harvey, C. D. (2017). Dynamic Reorganization of Neuronal Activity Patterns in Parietal Cortex. *Cell, 170*(5), 986-999 e916. doi:10.1016/j.cell.2017.07.021

Fanselow, M. S., & Dong, H. W. (2010). Are the dorsal and ventral hippocampus functionally distinct structures? *Neuron, 65*(1), 7-19. doi:10.1016/j.neuron.2009.11.031

Goode, T. D., Jin, J., & Maren, S. (2018). 10 - Neural Circuits for Fear Relapse. In S. Sangha & D. Foti (Eds.), *Neurobiology of Abnormal Emotion and Motivated Behaviors* (pp. 182-202): Academic Press.

Grewe, B. F., Grundemann, J., Kitch, L. J., Lecoq, J. A., Parker, J. G., Marshall, J. D., . . . Schnitzer, M. J. (2017). Neural ensemble dynamics underlying a long-term associative memory. *Nature, 543*(7647), 670-675. doi:10.1038/nature21682

Hainmueller, T., & Bartos, M. (2018). Parallel emergence of stable and dynamic memory engrams in the hippocampus. *Nature, 558*(7709), 292-296. doi:10.1038/s41586-018-0191-2

Hartley, N. D., Gaulden, A. D., Baldi, R., Winters, N. D., Salimando, G. J., Rosas-Vidal, L. E., . . . Patel, S. (2019). Dynamic remodeling of a basolateral-to-central amygdala glutamatergic circuit across fear states. *Nat Neurosci*. doi:10.1038/s41593-019-0528-7

Herry, C., Ciocchi, S., Senn, V., Demmou, L., Muller, C., & Luthi, A. (2008). Switching on and off fear by distinct neuronal circuits. *Nature, 454*(7204), 600-606. doi:10.1038/nature07166

Kearns, M. C., Ressler, K. J., Zatzick, D., & Rothbaum, B. O. (2012). Early interventions for PTSD: a review. *Depress Anxiety, 29*(10), 833-842. doi:10.1002/da.21997

Khalaf, O., Resch, S., Dixsaut, L., Gorden, V., Glauser, L., & Graff, J. (2018). Reactivation of recall-induced neurons contributes to remote fear memory attenuation. *Science, 360*(6394), 1239-1242. doi:10.1126/science.aas9875

Lacagnina, A. F., Brockway, E. T., Crovetti, C. R., Shue, F., McCarty, M. J., Sattler, K. P., . . . Drew, M. R. (2019). Distinct hippocampal engrams control extinction and relapse of fear memory. *Nat Neurosci, 22*(5), 753-761. doi:10.1038/s41593-019-0361-z

Liu, X., Ramirez, S., Pang, P. T., Puryear, C. B., Govindarajan, A., Deisseroth, K., & Tonegawa, S. (2012). Optogenetic stimulation of a hippocampal engram activates fear memory recall. *Nature, 484*(7394), 381-385. doi:10.1038/nature11028

Lopes-dos-Santos, V., Ribeiro, S., & Tort, A. B. (2013). Detecting cell assemblies in large neuronal populations. *J Neurosci Methods, 220*(2), 149-166. doi:10.1016/j.jneumeth.2013.04.010

Mankin, E. A., Sparks, F. T., Slayyeh, B., Sutherland, R. J., Leutgeb, S., & Leutgeb, J. K. (2012). Neuronal code for extended time in the hippocampus. *Proc Natl Acad Sci U S A, 109*(47), 19462-19467. doi:10.1073/pnas.1214107109

Maren, S. (2001). Neurobiology of Pavlovian fear conditioning. *Annu Rev Neurosci, 24*, 897-931. doi:10.1146/annurev.neuro.24.1.897

Maren, S. (2011). Seeking a spotless mind: extinction, deconsolidation, and erasure of fear memory. *Neuron, 70*(5), 830-845. doi:10.1016/j.neuron.2011.04.023

Maren, S. (2015). Out with the old and in with the new: Synaptic mechanisms of extinction in the amygdala. *Brain Res, 1621*, 231-238. doi:10.1016/j.brainres.2014.10.010

Mau, W., Sullivan, D. W., Kinsky, N. R., Hasselmo, M. E., Howard, M. W., & Eichenbaum, H. (2018). The Same Hippocampal CA1 Population Simultaneously Codes Temporal Information over Multiple Timescales. *Curr Biol, 28*(10), 1499-1508 e1494. doi:10.1016/j.cub.2018.03.051

Mukamel, E. A., Nimmerjahn, A., & Schnitzer, M. J. (2009). Automated analysis of cellular signals from large-scale calcium imaging data. *Neuron, 63*(6), 747-760. doi:10.1016/j.neuron.2009.08.009

Ramirez, S., Liu, X., Lin, P. A., Suh, J., Pignatelli, M., Redondo, R. L., . . . Tonegawa, S. (2013). Creating a false memory in the hippocampus. *Science, 341*(6144), 387-391. doi:10.1126/science.1239073

Ramirez, S., Liu, X., MacDonald, C. J., Moffa, A., Zhou, J., Redondo, R. L., & Tonegawa, S. (2015). Activating positive memory engrams suppresses depression-like behaviour. *Nature, 522*(7556), 335-339. doi:10.1038/nature14514

Rashid, A. J., Yan, C., Mercaldo, V., Hsiang, H. L., Park, S., Cole, C. J., . . . Josselyn, S. A. (2016). Competition between engrams influences fear memory formation and recall. *Science, 353*(6297), 383-387. doi:10.1126/science.aaf0594

Redondo, R. L., Kim, J., Arons, A. L., Ramirez, S., Liu, X., & Tonegawa, S. (2014). Bidirectional switch of the valence associated with a hippocampal contextual memory engram. *Nature, 513*(7518), 426-430. doi:10.1038/nature13725

Reijmers, L. G., Perkins, B. L., Matsuo, N., & Mayford, M. (2007). Localization of a stable neural correlate of associative memory. *Science, 317*(5842), 1230-1233. doi:10.1126/science.1143839

Reitich-Stolero, T., & Paz, R. (2019). Affective memory rehearsal with temporal sequences in amygdala neurons. *Nat Neurosci, 22*(12), 2050-2059. doi:10.1038/s41593-019-0542-9

Rescorla, R. A., & Heth, C. D. (1975). Reinstatement of fear to an extinguished conditioned stimulus. *J Exp Psychol Anim Behav Process, 1*(1), 88-96.

Resendez, S. L., Jennings, J. H., Ung, R. L., Namboodiri, V. M., Zhou, Z. C., Otis, J. M., . . . Stuber, G. D. (2016). Visualization of cortical, subcortical and deep brain neural circuit dynamics during naturalistic mammalian behavior with head-mounted microscopes and chronically implanted lenses. *Nat Protoc, 11*(3), 566-597. doi:10.1038/nprot.2016.021

Rubin, A., Geva, N., Sheintuch, L., & Ziv, Y. (2015). Hippocampal ensemble dynamics timestamp events in long-term memory. *Elife, 4*. doi:10.7554/eLife.12247

Rule, M. E., O'Leary, T., & Harvey, C. D. (2019). Causes and consequences of representational drift. *Curr Opin Neurobiol, 58*, 141-147. doi:10.1016/j.conb.2019.08.005

Ryan, T. J., Roy, D. S., Pignatelli, M., Arons, A., & Tonegawa, S. (2015). Memory. Engram cells retain memory under retrograde amnesia. *Science, 348*(6238), 1007-1013. doi:10.1126/science.aaa5542

Sheintuch, L., Rubin, A., Brande-Eilat, N., Geva, N., Sadeh, N., Pinchasof, O., & Ziv, Y. (2017). Tracking the Same Neurons across Multiple Days in Ca(2+) Imaging Data. *Cell Rep, 21*(4), 1102-1115. doi:10.1016/j.celrep.2017.10.013

Tanaka, K. Z., He, H., Tomar, A., Niisato, K., Huang, A. J. Y., & McHugh, T. J. (2018). The hippocampal engram maps experience but not place. *Science, 361*(6400), 392-397. doi:10.1126/science.aat5397

Tonegawa, S., Morrissey, M. D., & Kitamura, T. (2018). The role of engram cells in the systems consolidation of memory. *Nat Rev Neurosci, 19*(8), 485-498. doi:10.1038/s41583-018-0031-2

Tronson, N. C., Schrick, C., Guzman, Y. F., Huh, K. H., Srivastava, D. P., Penzes, P., . . . Radulovic, J. (2009). Segregated populations of hippocampal principal CA1 neurons mediating conditioning and extinction of contextual fear. *J Neurosci, 29*(11), 3387-3394. doi:10.1523/JNEUROSCI.5619-08.2009

Yiu, A. P., Mercaldo, V., Yan, C., Richards, B., Rashid, A. J., Hsiang, H. L., . . . Josselyn, S. A. (2014). Neurons are recruited to a memory trace based on relative neuronal excitability immediately before training. *Neuron, 83*(3), 722-735. doi:10.1016/j.neuron.2014.07.017

457 **Figure Legends**
458
459 **Figure 1.** Histological characterization of fear reinstatement schedule. (**a**) Behavioral design for
460 fear reinstatement. Mice underwent fear conditioning, and were then sacrificed at different points
461 in the behavioral schedule and had tissue stained for c-Fos. (**b**) Schematic of viral strategy. A
462 viral cocktail of AAV9-c-Fos-tTA and AAV9-TRE-eYFP was infused into the DG and BLA for
463 activity-dependent induction of eYFP. (**c**) Representative microscope image for the injection
464 sites. (**d**) Example confocal images of DG sections. Images from left to right: virus-labeled cells
465 (eYFP), c-Fos$^+$ cells (cFos), merged green and red channels (Merge). Yellow arrows designate
466 double-positive cells. Top images are representative of high overlap, and bottom are
467 representative of low overlap. (**e**) Same as **d** but for BLA sections. (**f**) Quantitative analysis of
468 overlap between FC-tagged BLA cells and c-Fos$^+$ BLA cells in each group. Overlap between
469 FC-tagged cells and c-Fos$^+$ cells was high after FC and there was a trending decrease following
470 EXT. Overlap remained low during the reinstating shock, but significantly increased during
471 Recall after reinstatement. (n = 15-27 sections per group, i.e. 5 mice per group and 2-11 sections
472 per mouse; $F_{3,88}$ =5.25; one-way ANOVA followed by Tukey's post-hoc test for pairwise
473 comparisons; #P < 0.1, *P < 0.05, **P < 0.01). Counts were normalized to % of eYFP$^+$ cells that
474 were also c-Fos$^+$. Small grey data points represent counts per section; big green data points
475 represent average counts per animal for **(f,h)**. (**g**) Correlation between average freezing during
476 Recall and overlap in the BLA demonstrates that overlap in the BLA is not predictive of freezing
477 (n = 15 mice; $F_{1,13}$ = 0.0209; ns P = 0.8873; R^2 = 0.0016; correlation). (**h**) Same as
478 quantification in **f**, but for DG. Overlap between FC-tagged cells and c-Fos$^+$ cells was high after
479 FC and significantly decreased following EXT. While overlap remained low during the
480 reinstating shock, it significantly increased during Recall after reinstatement. (n = 18-27 sections
481 per group, i.e. 4-6 mice and 2-6 sections per mouse; $F_{3,89}$ = 18.72; one-way ANOVA followed by
482 Tukey's post-hoc test for pairwise comparisons; **P < 0.01, ****P < 0.0001). (**i**) Correlation
483 between average freezing during Recall and overlap in the DG demonstrates that overlap in the
484 DG is predictive of freezing (n = 15 mice; $F_{1,13}$ = 6.374; *P = 0.0254; R^2 = 0.329; correlation).
485
486 **Figure 1 – figure supplement 1**. Behavior in reinstatement paradigm. (**a**) Mice underwent an 8-
487 minute fear conditioning session (FC), with four 1.5mA shocks spaced 80-seconds apart.
488 Compared to the first 3 minutes of FC (baseline freezing), mice froze significantly more in the
489 first three minutes of the EXT1 session (t_{15} = 11.858, ****P < 0.0001; paired t-test; n = 16
490 mice). (**b**) Mice underwent two 30-minute extinction sessions (EXT1 and EXT2) spaced 24
491 hours apart. Mice spent significantly less time freezing in the last three minutes of EXT2 as
492 compared to the first three minutes of EXT1 (t_{15} = 4.1631, ***P = 0.0008; paired t-test; n = 16
493 mice). (**c**) Following EXT, one group of mice was returned to the conditioned context for Recall
494 (EXT-Recall), while another group received an immediate shock in a novel context and was
495 removed 60-seconds later. After 24 hours, those mice were tested in the original conditioned
496 context for reinstatement (IS-Recall). (**d**) Compared to mice that did not receive the reinstating
497 shock, those that did showed significantly more freezing across a 5-minute Recall session (t_8 =
498 4.631, **P = 0.0017; unpaired t-test; n = 5 minutes for each group). (**e**) On average, mice that
499 received the reinstating shock froze significantly more during Recall than did mice that did not
500 receive the reinstating shock (t_6 = 4.018, **P = 0.0070; unpaired t-test; n = 4 mice per group). **(f)**
501 Quantification of relative numbers of eYFP+ cells across groups in the BLA (calculated as
502 #eYFP+ cells divided by area in arbitrary units). The EXT-Recall group had greater numbers of

503 eYFP+ cells in the BLA than the IS group did (n = 15-27 sections per group, i.e. 5 mice per
504 group and 2-11 sections per mouse; $F_{3,88}$ =3.777; one-way ANOVA followed by Tukey's post-
505 hoc test for pairwise comparisons; #P < 0.1, *P < 0.05). Small grey data points represent counts
506 per section; big green data points represent average counts per animal for **(f-i)**. **(g)** Quantification
507 of relative numbers of cFos+ cells across groups in the BLA (calculated as $cFos+ cells divided
508 by area in arbitrary units). The IS-Recall group expressed greater numbers of cFos+ cells than
509 did the EXT-Recall and IS groups (n = 15-27 sections per group, i.e. 5 mice per group and 2-11
510 sections per mouse; $F_{3,88}$ =3.444; one-way ANOVA followed by Tukey's post-hoc test for
511 pairwise comparisons; *P < 0.05). **(h)** Same as **(f)** but for DG. The IS group had greater relative
512 expression of eYFP+ cells than the the EXT-Recall group (n = 18-27 sections per group, i.e. 4-6
513 mice and 2-6 sections per mouse; $F_{3,89}$ = 2.814; one-way ANOVA followed by Tukey's post-hoc
514 test for pairwise comparisons; *P < 0.05). **(i)** Same as **(g)** but in DG. Expression of cFos+ cells in
515 the DG was stable across all groups (n = 18-27 sections per group, i.e. 4-6 mice and 2-6 sections
516 per mouse; $F_{3,89}$ = 1.216; one-way ANOVA).
517
518 **Figure 1 – figure supplement 2.** Reinstatement leads to partial generalization, but is largely
519 context-specific. (**a**) Behavioral design. Mice underwent the reinstatement as described in Figure
520 1; however, they were placed in the original conditioned context (context A) and a novel context
521 (context B), with some mice going into context A first and others context B first. (**b**) Compared
522 to freezing in the novel context, mice froze significantly more in the original conditioned context
523 across the 5-minute session (t_8 = 3.415, **P = 0.0092; unpaired t-test; n = 5 minutes for each
524 group).
525
526 **Figure 2**. BLA activity patterns change over extinction but resemble the fear conditioning state
527 during fear relapse. (**a**) Behavioral schedule for Ca^{2+} imaging cohort. (**b**) Left, freezing time
528 course of fear reinstatement paradigm (*n* = 6 mice). Right, pooled freezing. EXT1 vs. EXT2,
529 Wilcoxon signed-rank test *p* = 0.028; EXT2 vs Recall *p* = 0.046. Data are means ± standard error
530 of the mean. (**c**) Left, example field of view in BLA-implanted mouse, depicted as maximum
531 projection of CFC imaging session. Blue outlines indicate cell masks. Scale bar = 100 microns.
532 Right, fluorescence traces of 10 example cells (**d**) Pearson correlation coefficients between
533 population vectors during CFC and population vectors during EXT and Recall (*n* = 6 mice). Each
534 data point represents a measure of population similarity to CFC (30 s time bins). Two piecewise
535 regressions were fit each to EXT and Recall. (**e**) Box plots of population vector similarity
536 (predicted and empirical). Each data point represents a mouse's predicted r value (from the EXT
537 regression) for Recall compared to the actual observed r value during Recall (Shock context,
538 Wilcoxon signed-rank test *p* = 0.028; Neutral context, *p* = 0.46). (**f**) Groupings of neurons
539 (ensembles) were extracted from CFC, EXT1, and EXT2 using a previously published PCA/ICA
540 method (Lopes-dos-Santos et al., 2013). Averaged activations of those ensembles during Recall
541 were correlated with freezing during Recall (CFC ensemble during Recall, Pearson correlation *p*
542 = 0.007; EXT1 ensemble during Recall *p* = 0.04; EXT2 ensemble during Recall *p* = 0.80).
543
544 **Figure 2 – figure supplement 1.** Reemergence of CFC-associated brain activity during fear
545 relapse is specific to BLA and the shock context. (**a**) Left, correlation coefficients between EXT-
546 Recall and CFC population vectors in the shock context for BLA (*n* = 6 mice, duplicated from
547 Figure 2d). Right, predicted vs. empirical correlation values during Recall (duplicated from
548 Figure 2e). (**b**) Same as (**a**), but for CA1 (*n* = 6 mice). (**c**) Same as (**a**), but for the neutral context

549 (*n* = 4 mice). (**d**) Same as (**c**), but for CA1 (*n* = 4 mice). Wilcoxon signed-rank tests *p* = 0.028,
550 0.075, 0.46, 0.46 for **a-d** respectively.
551
552 **Figure 2 – figure supplement 2.** Cell registration examples. (**a**) Registration diagnostics for
553 example CA1 Ca^{2+} imaging mouse. Top, cell centroids pre-alignment. Middle, cell centroids
554 post-alignment. Colors correspond to different sessions. Bottom, 2-dimensional histogram of
555 matched pairs. Note the high density of cells within 3 microns of their match on another session.
556 (**b**) Same as (**a**), but for example BLA mouse. Figures were modified from plots generated via
557 software from Sheintuch et al., 2017.
558
559 **Figure 3.** Optical inhibition of the DG or BLA fear ensemble disrupts reinstated fear. (**a**)
560 Schematic of viral strategy. A virus cocktail of AAV9-c-Fos-tTA and AAV9-TRE-ArchT-eYFP
561 was infused into either the DG or BLA for activity-dependent expression of ArchT-eYFP. (**b**)
562 Representative microscope images of injection sites for the DG and BLA groups of mice. (**c**)
563 Reinstatement behavioral schedule. Mice had the fear ensemble labeled in either the DG or BLA
564 and inhibited during Recall after Shock Reinstatement. (**d-g**) Line graphs: 2-minute light OFF
565 and ON epochs during Recall for the two experimental ArchT groups (DG Exp & BLA Exp) and
566 the two control no-opsin groups (DG eYFP & BLA eYFP). Bar graphs: Quantification of
567 average freezing between light OFF vs. light ON epochs for each group. (**d)** DG Exp Recall (t_{24}
568 = 2.781, *P = 0.0104; paired t-test; n = 25 paired epochs from 13 mice). (**e**) BLA EXP Recall (t_{17}
569 = 4.277, ***P = 0.0005; paired t-test; n = 18 paired epochs from 9 mice). (**f**) DG eYFP Recall
570 (t_{21} = 0.05067, n.s., P = 0.9600; paired t-test; n = 22 paired epochs from 11 mice). (**g**) BLA eYFP
571 Recall (t_{15} = 0.3915, n.s., P = 0.7010; paired t-test; n = 16 paired epochs from 8 mice). (**h**)
572 Behavioral schedule to test for specificity of DG and BLA fear ensemble in disrupting
573 reinstatement-induced fear. Mice had cells active during Female Exposure labeled in either the
574 DG or BLA, and then underwent FC, EXT, Shock Reinstatement, and had the labeled cells
575 inhibited during Recall. (**i,j**) Same line and bar graphs as in **d-g**, but for the behavioral design in
576 h. (**i**) DG Pos Recall (t_{23} = 2.053, n.s., P = 0.0516; paired t-test; n = 24 paired epochs from 12
577 mice). (**j**) BLA Pos Recall (t_{15} = 0.1986, n.s., P = 0.8452; paired t-test; n = 16 paired epochs from
578 8 mice). (**k**) Freezing difference scores across the three DG groups (Exp, Pos, eYFP), calculated
579 as freezing in light ON epoch – freezing in light OFF epoch, for each set of epochs for each
580 mouse. There was a strong trend towards a decrease in freezing in the light ON epoch in the Exp
581 group vs. the eYFP group, and there was no difference in the Pos vs. eYFP groups (from left to
582 right: n = 25 scores from 13 mice, 24 scores from 12 mice, 22 scores from 11 mice; $F_{2,68}$ = 2.351,
583 P = 0.1030; DG Exp vs. DG eYFP, n.s., P = 0.0658; DG Pos vs. DG eYFP, n.s., P = 0.2682; one-
584 way ANOVA followed by Dunnett's test). (**l**) Same as **k** but for BLA groups. The BLA Exp
585 group showed significantly lower freezing during the light ON epoch compared to the BLA
586 eYFP group (*p* = 0.0122), whereas there was no difference in the BLA Pos vs. BLA eYFP
587 groups (*p* = 0.8797) (from left to right: n = 18 scores from 9 mice, 16 scores from 8 mice, 16
588 scores from 8 mice; $F_{2,47}$ = 4.811, P = 0.0126; BLA Exp vs. BLA eYFP, *P = 0.0122; BLA Pos
589 vs. BLA eYFP, n.s., P = 0.8797; one-way ANOVA followed by Dunnett's test). (**m**) Summary
590 graph of freezing difference scores across all groups in Figure 3. While mice in the BLA and DG
591 Exp groups show significantly less freezing during light ON epochs, the BLA and DG Pos
592 groups and BLA and DG eYFP groups show no difference in freezing between light ON and
593 light OFF epochs (from left to right: n = 18 scores from 9 mice, 25 scores from 13 mice, 16
594 scores from 8 mice, 24 scores from 12 mice, 16 scores from 8 mice, 22 scores from 12 mice;

BLA Exp, $t_{17} = 4.277$, ***P = 0.0005; DG Exp, $t_{24} = 2.781$, *P = 0.0104; BLA Pos, $t_{15} = 0.1986$, n.s., P = 0.8452; DG Pos, $t_{23} = 2.053$, n.s., P = 0.0516; BLA eYFP, $t_{15} = 0.3915$, n.s., P = 0.7010; DG eYFP, $t_{21} = 0.05076$, n.s., P = 0.9600; one-sample t-tests, $\mu_0 = 0$).

Figure 3 – figure supplement 1. Inhibition of BLA fear ensemble does not prevent reinstatement. **(a)** Schematic of viral strategy. A viral cocktail of AAV9-c-Fos-tTA and AAV9-TRE-ArchT-eYFP was infused into the BLA for activity-dependent induction of ArchT-eYFP. **(b)** Representative microscope image of BLA injection site. Dotted line indicates optic fiber placement. **(c)** Behavioral schedule to test if inhibition of BLA fear ensemble during Shock Reinstatement can prevent reinstatement. **(d)** Left: Freezing during fear conditioning and extinction. Upper right: Compared to the first 3 minutes of FC (baseline freezing), mice froze significantly more in the first three minutes of the EXT1 session ($t_{10} = 17.112$, ****P < 0.0001; paired t-test; n = 10 mice). Bottom right: Mice spent significantly less time freezing in the last three minutes of EXT2 as compared to the first three minutes of EXT1 ($t_{10} = 5.5159$, ***P = 0.0003; paired t-test; n = 10 mice). **(e)** Compared to no-opsin controls (eYFP group), experimental mice that received optical inhibition (ArchT group) showed comparable levels of freezing during Recall, indicating that inhibition of the BLA fear ensemble did not prevent reinstatement ($t_9 = 0.935$, n.s., P = 3742; unpaired t-test; ArchT, n = 7 mice; eYFP, n = 4 mice).

Figure 3 – figure supplement 2. Stimulation of BLA or DG fear ensemble does not mimic reinstatement. (**a**) Behavioral schedule to test if stimulation of BLA fear ensemble in a novel environment can mimic reinstatement. (**b**) Left: Freezing during fear conditioning and extinction for BLA-implanted animals. Middle: Compared to the first 3 minutes of FC (baseline freezing), mice froze significantly more in the first three minutes of the EXT1 session ($t_{15} = 17.171$, ****P < 0.0001; paired t-test; n = 16 mice). Right: Mice spent significantly less time freezing in the last three minutes of EXT2 as compared to the first three minutes of EXT1 ($t_{15} = 7.9973$, ****P < 0.0001; paired t-test; n = 16 mice). (**c**) Left: Freezing during fear conditioning and extinction for DG-implanted animals. Middle: Compared to the first 3 minutes of FC (baseline freezing), mice froze significantly more in the first three minutes of the EXT1 session ($t_{15} = 13.238$, ****P < 0.0001; paired t-test; n = 16 mice). Right: Mice spent significantly less time freezing in the last three minutes of EXT2 as compared to the first three minutes of EXT1 ($t_{15} = 5.9671$, ****P < 0.0001; paired t-test; n = 16 mice). (**d**) Left: Freezing across Recall session after BLA fear ensemble stimulation for ChR2 and eYFP groups. Right: Comparison of average freezing during Recall session after BLA fear ensemble stimulation, for ChR2 and eYFP groups ($t_{14} = 0.8265$, n.s., P = 0.4224; unpaired t-test; n = 8 mice in each group). (**e**) Left: Freezing across Recall session after DG fear ensemble stimulation for ChR2 and eYFP groups. Comparison of average freezing during Recall session after DG fear ensemble stimulation, for ChR2 and eYFP groups ($t_{14} = 1.522$, n.s., P = 0.1503; unpaired t-test; n = 8 mice in each group).

Figure 3 – figure supplement 3. Inhibition of the fear ensemble after extinction does not alter freezing behavior. (**a**) Behavioral design. Mice underwent FC and two EXT sessions, followed by an 8-minute Recall session, with 2-minute light OFF/light ON epochs. (**b**) Left: Freezing during fear conditioning and extinction. Middle: Compared to the first 3 minutes of FC (baseline freezing), mice froze significantly more in the first three minutes of the EXT1 session ($t_{15} = 25.898$, ****P < 0.0001; paired t-test; n = 16 mice). Right: Mice spent significantly less time freezing in the last three minutes of EXT2 as compared to the first three minutes of EXT1 ($t_{15} =$

9.7348, ****P < 0.0001; paired t-test; n = 16 mice). (**c-e**) Line graphs: 2-minute light OFF and ON epochs during Recall for the two experimental ArchT groups (DG ArchT & BLA ArchT) and the one control no-opsin group (DG eYFP). Bar graphs: Quantification of average freezing between light OFF vs. light ON epochs for each group. (**c**) DG ArchT Recall (t_{11} = 1.65, n.s., P = 0.1273; paired t-test; n = 12 paired epochs from 6 mice). (**d**) DG eYFP Recall (t_7 = 0.4724, n.s., P = 0.6510; paired t-test; n = 8 paired epochs from 4 mice). (**e**) BLA ArchT Recall (t_{11} = 0.9078, n.s., P = 0.3835; paired t-test; n = 12 paired epochs from 6 mice). (**f**) Summary graph of freezing difference scores across all graphs in this figure, calculated as freezing in light ON epoch – freezing in light OFF epoch, for each set of epochs for each mouse. There was no significant difference in freezing between the DG ArchT and DG eYFP groups (t_{18} = 0.8689, n.s., P = 0.3963; unpaired t-test; DG ArchT, n = 12 scores from 6 mice; DG eYFP, n = 8 scores from 4 mice).

687 **Methods**
688
689 *Subjects*
690 Wildtype male C57BL/6 mice (6-8 weeks of age; Charles River Labs) were housed in
691 groups of 4-5 mice per cage. The animal facilities (vivarium and behavioral testing rooms) were
692 maintained on a 12:12-hour light cycle (lights on at 0700). Mice were placed on a diet containing
693 40 mg/kg doxycycline (Dox) for a minimum of two days before receiving surgery with access to
694 food and water *ad libitum*. Mice recovered for at least ten days after surgery. Dox-containing diet
695 was replaced with standard mouse chow (*ad libitum*) 48 hours prior to behavioral tagging to
696 open a time window of activity-dependent labeling (Ramirez et al., 2013).
697 All procedures relating to mouse care and treatment conformed to the institutional and
698 National Institutes of Health guidelines for the Care and Use of Laboratory Animals. No
699 statistical methods were used to predetermine sample size; however, sample sizes were chosen
700 based on sample sizes in previous studies (Ramirez et al., 2013). Data collection and analysis
701 were not performed blind to the conditions of the experiments.
702
703 Activity-dependent viral constructs
704 $pAAV_9$-cFos-tTA, $pAAV_9$-TRE-eYFP, and pAAV 9 -TRE-ArchT-eYFP were constructed as
705 previously described(Ramirez et al., 2015). $pAAV_9$-c-Fos-tTA was combined with $pAAV_9$-TRE-
706 eYFP or $pAAV_9$-TRE-ArchT-eYFP prior to injection at a 1:1 ratio.
707
708 Stereotaxic surgeries
709 *Opsin injections and optic fiber implants*: Stereotaxic injections and optical fiber
710 implants followed methods previously reported(Ramirez et al., 2015). All surgeries were
711 performed under stereotaxic guidance and subsequent coordinates are given relative to Bregma
712 (in mm). Mice were mounted into a stereotaxic frame (Kopf Instruments, Tujunga, CA, USA)
713 and anesthetized with 3% isoflurane during induction and lowered to 1-2% to maintain
714 anesthesia (oxygen 1L/min) throughout the surgery. Ophthalmic ointment was applied to both
715 eyes to prevent corneal desiccation. Hair was removed with scissors and the surgical site was
716 cleaned with ethanol and betadine. Following this, an incision was made to expose the skull.
717 Bilateral craniotomies involved drilling windows through the skull above the injection sites using
718 a 0.5 mm diameter drill bit. Coordinates were -1.35mm anteroposterior (AP), ±3.45mm
719 mediolateral (ML), and -5.15mm dorsoventral (DV) for basolateral amygdala (BLA)(Davis et
720 al., 2017); and -2.2mm AP, ±1.3mm ML, and -2.0mm DV for dorsal dentate gyrus
721 (dDG)(Ramirez et al., 2015). All mice were injected with a volume of 0.3 µl of AAV9 cocktail
722 per site at a control rate of 0.1 µl min^{-1} using a mineral oil-filled 33-gage beveled needle attached
723 to a 10 µl Hamilton microsyringe (701LT; Hamilton) in a microsyringe pump (UMP3; WPI).
724 The needle remained at the target site for two minutes post-injection before removal. For dDG
725 optogenetic experiments, a bilateral optic fiber implant (200 µm core diameter; Doric Lenses)
726 was chronically implanted above the injection site (-1.6mm DV). For BLA optogenetic
727 experiments, monofibers were implanted above each injection site (-4.9mm DV). Jewelry screws
728 secured to the skull acted as anchors. Layers of adhesive cement (C&B Metabond) followed by
729 dental cement (A-M Systems) were spread over the surgical site. Mice that did not receive
730 implants had their incision sutured. Mice received 0.1 mL of 0.3 mg/ml buprenorphine
731 (intraperitoneally) following surgery and were placed on a heating pad during recovery.

732 *GCaMP6f injections and lens implants*: Mice in Ca^{2+} imaging experiments underwent
733 three separate serial surgeries. First, mice received unilateral infusions of AAV9-Syn-GCaMP6f
734 (U Penn Vector Core) into either right CA1 (AP -2.0 mm, ML +1.5 mm, DV -1.5 mm) or right
735 BLA (AP -1.35 mm, ML +3.45 mm, DV -5.05 mm). The viral vector was injected at a rate of 40
736 nL/min and allowed 10 min to diffuse before the scalp was sutured.
737 Two to four weeks after viral infusion, mice were implanted with a gradient index
738 (GRIN) lens into either CA1 (1 mm diameter, 4 mm length, Inscopix; AP -2.25 mm, ML +1.8
739 mm, DV -1.3 mm) or BLA (0.65 mm diameter, 7.3 mm length; AP -1.25 mm, ML +3.15 mm,
740 DV -4.85 mm). For CA1 implants, overlying neocortex was aspirated under continuous irrigation
741 with cold 0.9% saline until vertical white fibers were visible (Resendez et al., 2016). For BLA
742 implants, a tract was created using a stereotaxically lowered 27-gauge needle (0.5 mm diameter)
743 into the craniotomy prior to insertion of the lens. Gaps between the lens and the skull were filled
744 using Kwik-Sil (World Precision Instruments) and the lens was then adhered to the skull using
745 Metabond. The surface of the lens was covered with a protective cap made of Kwik-Cast (World
746 Precision Instruments) until base plate attachment.
747 Finally, one week after the lens implant, mice were implanted with a base plate for
748 microscope attachment. A plastic base plate was magnetically attached to the bottom of the
749 microscope. The microscope objective was then aligned to the GRIN lens and lowered until cells
750 came into focus, as observed via nVista recording software (Inscopix). The base plate was then
751 adhered to the surrounding Metabond on the animal's skull using a dental composite (Flow-It
752 ALC, Pentron) and strengthened with an additional layer of Metabond.
753 Histological assessment verified viral targeting and fiber/lens placement. Data from off-
754 target injections and implants were not included in analyses.
755
756 Optogenetic methods
757 Optic fiber implants were plugged into a patch cord connected to a 520nm green laser
758 diode controlled by automated software (Doric Lenses). Laser diode output was tested at the
759 beginning of every experiment to ensure that at least 10 mW of power was delivered at the end
760 of the optic fiber tip (Doric lenses). Mice began the stimulation trial with a 2-min light-off epoch,
761 followed by 2-min optical stimulation (15 ms pulse width, 20 Hz), and then repeated, such that
762 the mice underwent a light-OFF/ON/OFF/ON pattern for a total of 8-min.
763
764 Behavioral tagging
765 Dox diet was replaced with standard lab chow (*ad libitum*) 48-hours prior to behavioral
766 tagging. *Female exposure*: One female mouse (PD 30-40) was placed into a clean home cage
767 with a clear cage top, which was used as the interaction chamber. The experimental male mouse
768 was then placed into the chamber and allowed to interact freely for one hour(Ramirez et al.,
769 2015). *Fear conditioning*: Mice were placed into a conditioning chamber and received fear
770 conditioning (see below) over a 500-second training session (including exposure to four 1.5 mA
771 foot shocks). Following behavioral tagging, the male mouse was returned to their home cage
772 with access to Dox diet (Ramirez et al., 2013).
773
774 Behavior
775 All behavior assays were conducted during the light cycle of the day (0730–1930). Mice
776 were handled for 1-2 days, 2 min per day, before all behavioral experiments, and were run by
777 cage. The entire behavioral schedule includes female exposure, fear conditioning, extinction,

reinstatement, and recall (described below). Which of these behaviors the mice underwent depended on the experiment.

Female exposure: One female mouse (PD 30-40) was placed into a clean home cage with a clear cage top and no bedding, which was used as the interaction chamber. The experimental male mouse was then placed into the chamber and allowed to interact freely for one hour(Ramirez et al., 2015).

Fear conditioning: Fear conditioning occurred in one of four mouse conditioning chambers (Coulbourn Instruments, Whitehall, PA, USA) with metal-panel side walls, Plexiglas front and rear walls, and a stainless-steel grid floor composed of 16 grid bars. The grid floor was connected to a precision animal shocker (Coulbourn Instruments, Whitehall, PA, USA) set to deliver a 2-second 1.5 mA foot shock unconditioned stimulus (US). A ceiling-mounted video camera recorded activity and fed into a computer running FreezeFrame3 software (Actimetrics, Wilmette, IL, USA). The software controlled stimuli presentations and recorded videos from four chambers simultaneously. The program determined movement as changes in pixel luminance. Context alterations included changes to spatial, olfactory, tactile, and lighting cues. The conditioning chamber with room lights off was designated as Context A. Context B involved modifications to the conditioning chamber, including vertical black and white strips spaced ~ 3 cm apart obscuring the front and rear walls, black inserts placed between grids to slightly alter dimensions of the box, 1 mL of almond extract in a plastic container positioned below the grid floor, and room lights on. Context C also involved modifications to the conditioning chamber, with a plastic sheet with a cross-hatch texture placed over the shock grid to change tactile cues, a black sheet obscuring the front walls, 1 mL of orange extract in a plastic container position below the grid floor, and room lights on. The chambers were cleaned with 70% ethanol solution prior to animal placement. Contextual fear conditioning occurred in Context A. Briefly, mice were placed into the conditioning context for a 500-second acquisition session, including a 180-second baseline period followed four 1.5 mA, 2-second foot shock USs (interstimulus interval [ISI] equals 80-sec). In optogenetic experiments, mice had patch cords attached near the conditioning chamber by the experimenter, and were run two mice at a time.

Fear conditioning data are collected using FreezeFrame3 software (Actimetrics, Wilmette IL) with the bout length set at 1.25-sec and the freezing threshold initially set as described in the program instructions. Freezing is defined as changes in pixel luminance falling below a threshold. An experimenter adjusted the threshold so that freezing behavior involves the absence of all movement except those needed for respiration as previously described. Freezing behavior was scored as the percentage of time spent freezing during a given bout of time. Statistical analyses involved paired t-tests comparing within subject differences (i.e. light off vs light on epochs), unpaired t-tests comparing across experimental groups (e.g. ArchT group vs. eYFP group), and one-sample t-tests comparing freezing differences scores to a $\mu_0 = 0$.

Extinction: Extinction occurred in Context A (described above) the day following fear conditioning. Mice were placed in Context A for 30-min sessions once per day, for two days. As in fear conditioning, cages of four mice were run simultaneously, and cages of five mice were run as three mice first, then the remaining two.

Reinstatement: Reinstatement occurred in Context B (described above) the day following the second day of extinction. Mice were placed in Context B and given a 1.5 mA, 2-second foot shock 1-second into the trial. Mice were left in the chamber for another 60-seconds before being removed. As opposed to being run four mice simultaneously as in fear conditioning and extinction, each mouse in a cage was run individually for reinstatement.

824 *Recall*: Recall for behavioral and overlap experiments involved placement in a context
825 for 5-min. In this case, as in fear conditioning and extinction, cages of four mice were run
826 simultaneously while cages of five mice were run as three mice first, then the remaining two. In
827 optogenetic experiments, recall involved an 8-min session consisting of 2-min epochs of
828 alternating light off and light on. In this case, mice were run one or two at a time.
829
830 Immunohistochemistry.
831 Mice were anesthetized with 3% isoflurane and perfused transcardially with cold (4° C)
832 phosphate- buffered saline (PBS) followed by cold 4% paraformaldehyde (PFA) in PBS. Brains
833 were extracted and stored overnight in PFA at 4°C. Fifty µm coronal sections were collected in
834 serial order using a vibratome and collected in cold PBS (100 µm coronal sections were collected
835 when solely verifying injection site and implant placement). Immunostaining involved washing
836 sections in PBS with 0.2% triton (PBST) for 10-minutes (x3). Sections were blocked for 1 hour
837 at room temperature in PBST and 5% normal goat serum (NGS) on a shaker. Sections were
838 transferred to wells containing primary antibodies (1:5000 rabbit anti-c-Fos [SySy]; 1:500
839 chicken anti-GFP [Invitrogen]) and allowed to incubate on a shaker overnight at 4°C. Sections
840 were then washed in PBST for 10-min (x3), followed by 2-hour incubation with secondary
841 antibody (1:200 Alexa 555 anti-rabbit [Invitrogen]; 1:200 Alexa 488 anti-chicken [Invitrogen]).
842 Following three additional 10-min washes in PBST, sections were mounted onto micro slides
843 (VWR International, LLC). Vectashield Hard Set Mounting Medium with DAPI (Vector
844 Laboratories, Inc) was applied, slides were cover slipped, and allowed to dry overnight.
845
846 Cell counting.
847 The number of eYFP- or cFos-immunoreactive neurons in the dentate gyrus and
848 basolateral amygdala were counted to measure the number of active cells during defined
849 behavioral tasks per mouse. Only animals that had accurate injections were selected for counting,
850 and sections closest to the injection coordinates for each brain region were chosen (see the
851 Stereotaxic surgeries section of Methods). All animals were sacrificed 90 minutes post-assay for
852 immunohistochemical analyses. Fluorescence images were acquired using a confocal microscope
853 (Zeiss LSM800, Germany) with a 10X objective for dentate gyrus images and 20X objective for
854 basolateral amygdala images. Z-stacked images were taken at step sizes of 3um for DG and
855 1.54um for BLA in the z-axis and maximum projections of these z-stacks were taken for
856 counting.
857 For the dentate gyrus, the number of eYFP-positive and cFos-positive cells in a set region
858 of interest were quantified manually using ImageJ. eYFP positive cells in the basolateral
859 amygdala were quantified automatically using a custom Python script that detects cells based on
860 size and circularity of objects in an image, while cFos-positive cells were quantified manually
861 with ImageJ because of poorer signal to noise in cFos images compared with the eYFP images.
862 To calculate the percentage of re-activated cells we counted the number of eYFP-positive
863 cells, cFos-positive cells, and both eYFP- and cFos-positive (Overlapped) cells. Re-activation
864 was calculated as (Overlap/eYFP*100). Overlap was compared across groups using unpaired t-
865 test (two-groups) and one-way ANOVA (more than two groups). Relative expression of eYFP
866 and cFos across groups was calculated as (#eYFP cells/Area) and (#cFos cell/Area) in arbitrary
867 area units.
868
869 *In vivo* calcium imaging

870 A miniaturized microscope (Inscopix) was used to collect Ca^{2+} imaging videos in mice
871 undergoing the fear reinstatement schedule. Videos were captured using nVista (Inscopix) at 20
872 Hz in a 720 x 540 pixel field of view (1.1 microns/pixel). Microscope attachments were done
873 while the mice were awake and restrained.
874 Ca^{2+} imaging videos were cropped, spatially bandpass filtered, and motion corrected
875 offline using Inscopix Data Processing Software v1.1. A ΔF/F movie was computed using the
876 mean fluorescence of the movie as the baseline and PCA/ICA was used for automated
877 segmentation of cell masks (Mukamel, Nimmerjahn, & Schnitzer, 2009). PCA/ICA putative cell
878 masks were each manually inspected to verify that cells were accurately captured with high
879 fidelity. Cells across imaging sessions were aligned and registered to each other using the
880 automated CellReg software in Matlab (Sheintuch et al., 2017).
881 Population vectors (PVs) were computed for the entirety of the CFC session by taking the
882 average Ca^{2+} transient rate for each cell while the mouse was in the fear conditioning chamber.
883 PVs for EXT1, EXT2, and Recall were defined as the average Ca^{2+} transient rate for each 30 s
884 time bin while the mouse was in the chamber. As a measure of the similarity of the population to
885 the CFC network state, Pearson correlations were performed between each 30 s PV to the CFC
886 PV. As a control, we also performed correlations between PVs from a neutral context to the CFC
887 PV. Only cells that were active for both sessions being correlated (CFC and either EXT1, EXT2,
888 or Recall) were considered.
889 We used piecewise regressions to determine whether reinstatement increased PV
890 correlations (to CFC) greater than would be expected from chance. For each mouse, we fit PV
891 correlation coefficients using time as a predictor for the EXT sessions and the Recall session
892 separately. Next, using the regression models obtained from the EXT session data, we predicted
893 the PV correlation value that should be observed during the first time bin in Recall. Then we
894 compared the predicted values to the actual values derived from the y-intercepts of the regression
895 models on the Recall data.
896
897 Neuronal Ensembles
898 We characterized neuronal ensembles from Ca^{2+} transient activity and correlated their
899 later activity during Recall to relapse-associated freezing. To extract neuronal ensembles, we
900 used a PCA/ICA method that was previously published (Lopes-dos-Santos et al., 2013). This
901 method is a source separation algorithm that is similar in principle to the PCA/ICA that was run
902 on Ca^{2+} imaging movies earlier (Mukamel et al., 2009). However, rather than extracting neurons
903 from pixel fluorescence, we are now extracting ensembles from traces. First, Ca^{2+} traces were z-
904 score normalized. Then, principal components analysis (PCA) was used to reduce the
905 dimensionality of the trace matrix and to compute eigenvalues corresponding to the variances
906 along the reduced dimensions. To produce a surrogate dataset for determining significant
907 eigenvalues, we circularly shuffled each neuron's Ca^{2+} trace vector and performed PCA on that
908 shuffled data 1000 times. Next, significant ensembles were tallied based on eigenvalues
909 exceeding a statistically defined threshold (eigenvalues must be > 99% of all the eigenvalues
910 computed from the PCA of the shuffled data). To extract statistically independent ensembles, an
911 independent components analysis (ICA) was run on the trace matrix with the number of
912 components specified by the number of statistically significant ensembles (eigenvalues). From
913 this computation, each ensemble now has a corresponding "pattern" vector describing the weight
914 of each neuron contributing to that ensemble. For each ensemble, a projection matrix was
915 computed from the outer product of these pattern vectors with the identity of the matrix set to 0

(to ensure that more than one neuron was needed to trigger an ensemble activation). The projection matrix was multiplied with each observation (frame) of the trace matrix to obtain ensemble activation strength. Finally, an ensemble was considered to be significantly activated if it exceeded 2 standard deviations above its mean activation strength.

Ensembles were extracted individually for CFC, EXT1, and EXT2. Only neurons that were active between these sessions and Recall were considered. After ensembles were extracted, their activity strength during Recall was calculated and the proportion of significant activations was correlated with freezing.

Data Analysis.

Data were analyzed using Inscopix nVista in conjunction with custom-made R, Python, and Matlab scripts. Data were analyzed using paired t-tests (two factors) or with one-way and repeated measures ANOVAs (more than two factors), Wilcoxon signed-rank tests, and Mann-Whitney U tests (two-tailed, corrected for multiple comparisons using false discovery rate adjustments). Post-hoc analyses (Tukey's) were used to characterize treatment and interaction effects, when statistically significant (alpha set at $p<0.05$, two-tailed).

Figure 1

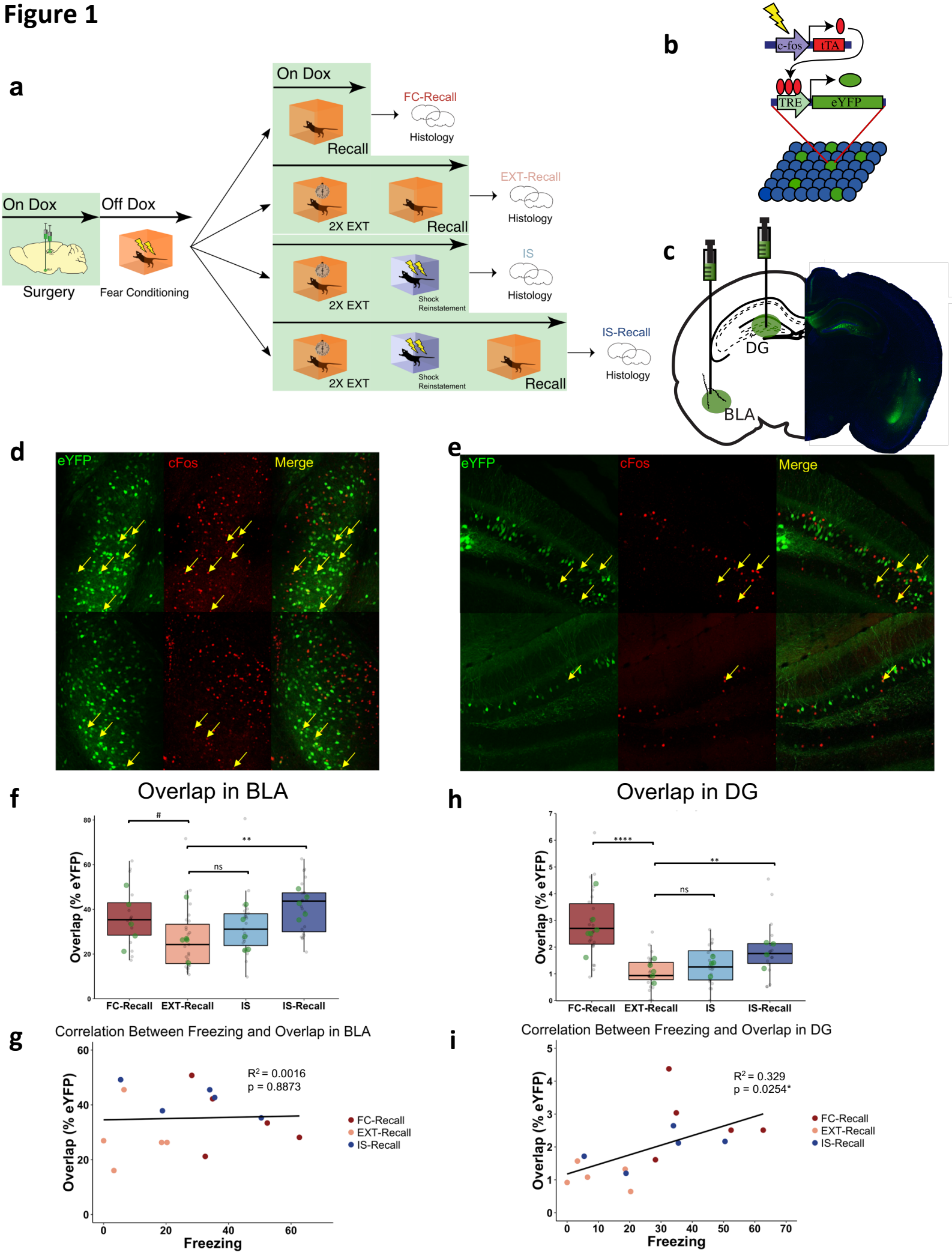
a
On Dox
Off Dox
Surgery
Fear Conditioning
On Dox
Recall
FC-Recall
Histology
2X EXT
Recall
EXT-Recall
Histology
2X EXT
Shock Reinstatement
IS
Histology
2X EXT
Shock Reinstatement
Recall
IS-Recall
Histology
b
c-fos
tTA
TRE
eYFP
c
DG
BLA
d
eYFP
cFos
Merge
e
eYFP
cFos
Merge
f
Overlap in BLA
Overlap (% eYFP)
FC-Recall
EXT-Recall
IS
IS-Recall
h
Overlap in DG
Overlap (% eYFP)
FC-Recall
EXT-Recall
IS
IS-Recall
g
Correlation Between Freezing and Overlap in BLA
R2 = 0.0016
p = 0.8873
Overlap (% eYFP)
Freezing
FC-Recall
EXT-Recall
IS-Recall
i
Correlation Between Freezing and Overlap in DG
R2 = 0.329
p = 0.0254*
Overlap (% eYFP)
Freezing
FC-Recall
EXT-Recall
IS-Recall

Figure 1 – figure supplement 1

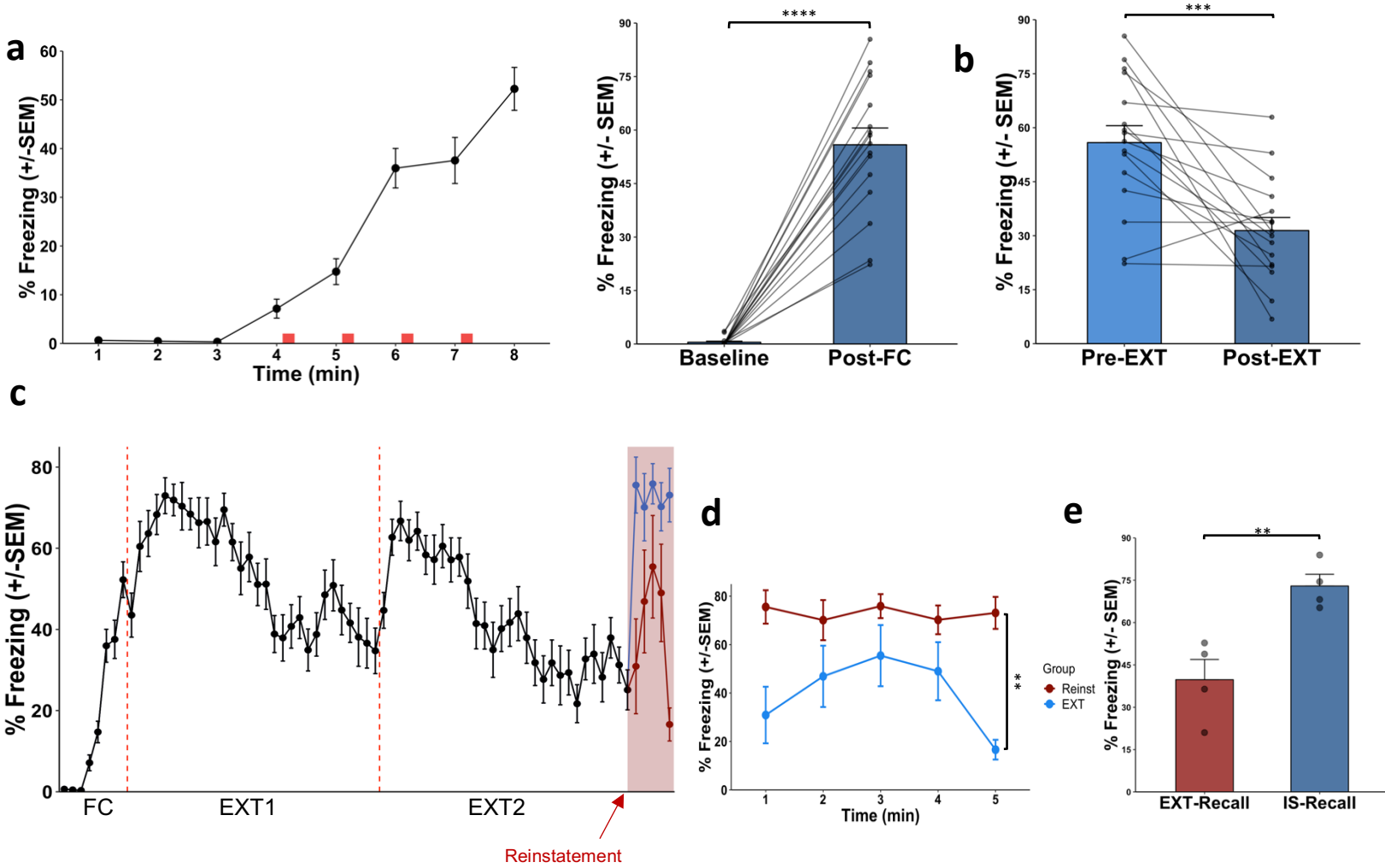

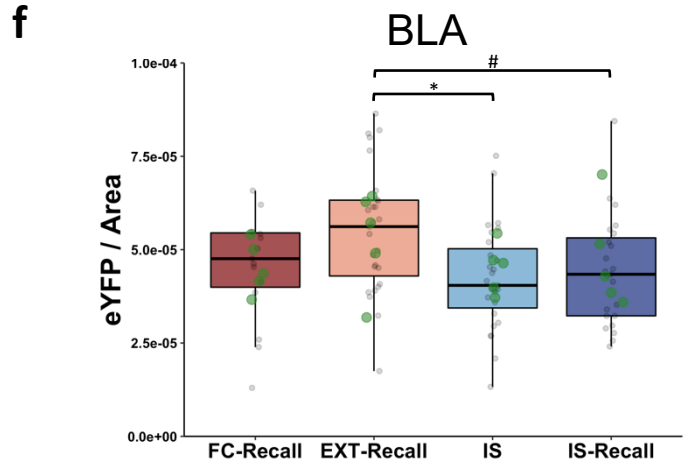

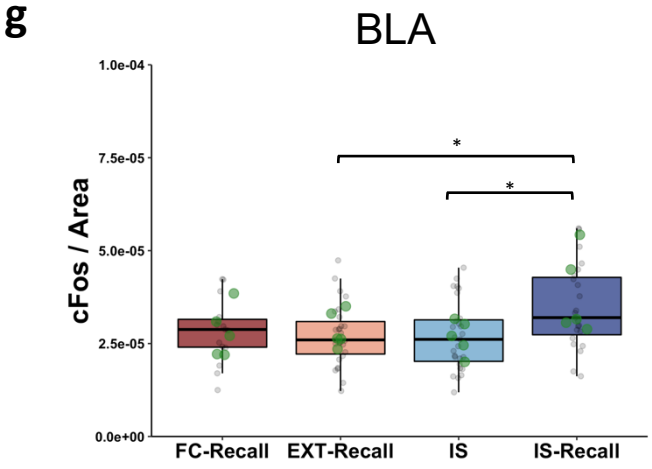

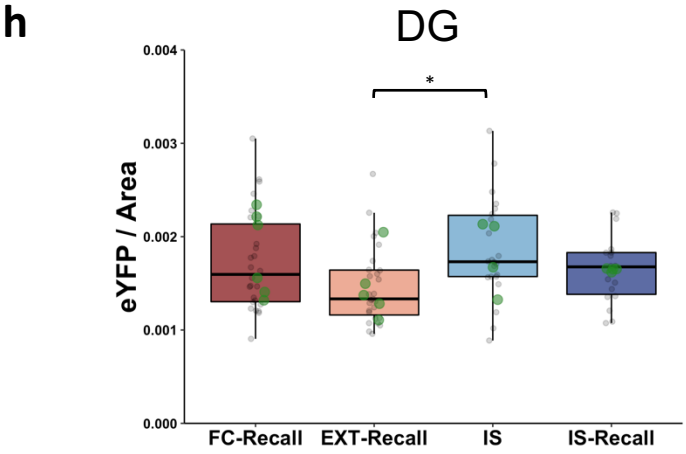

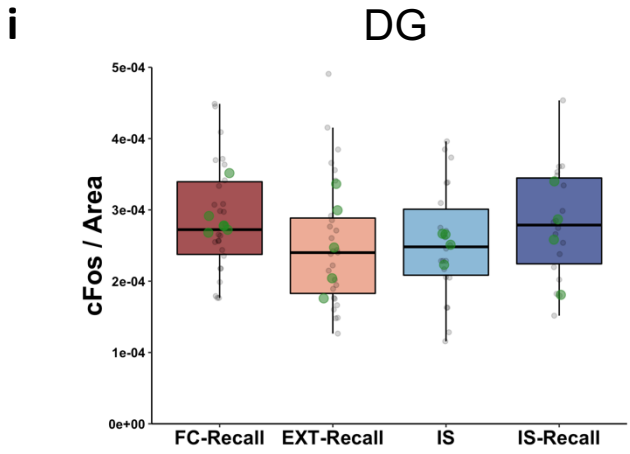

Figure 1 – figure supplement 2

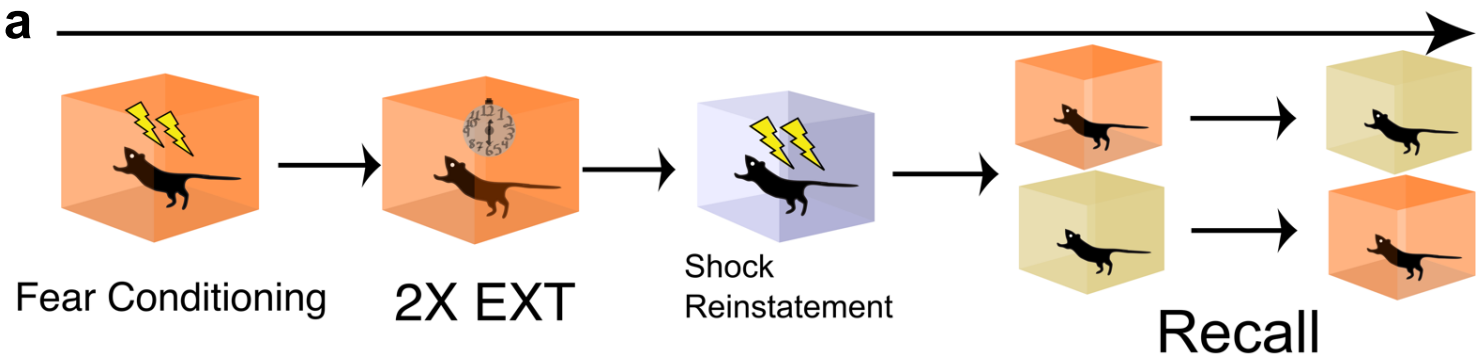

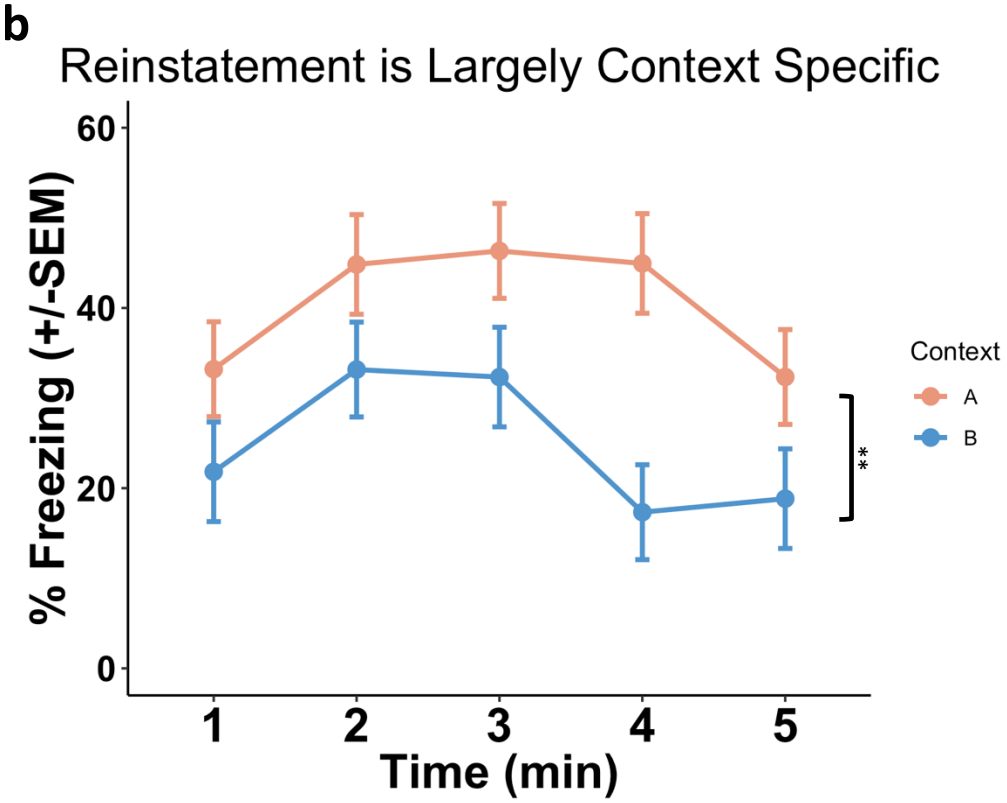

Figure 2

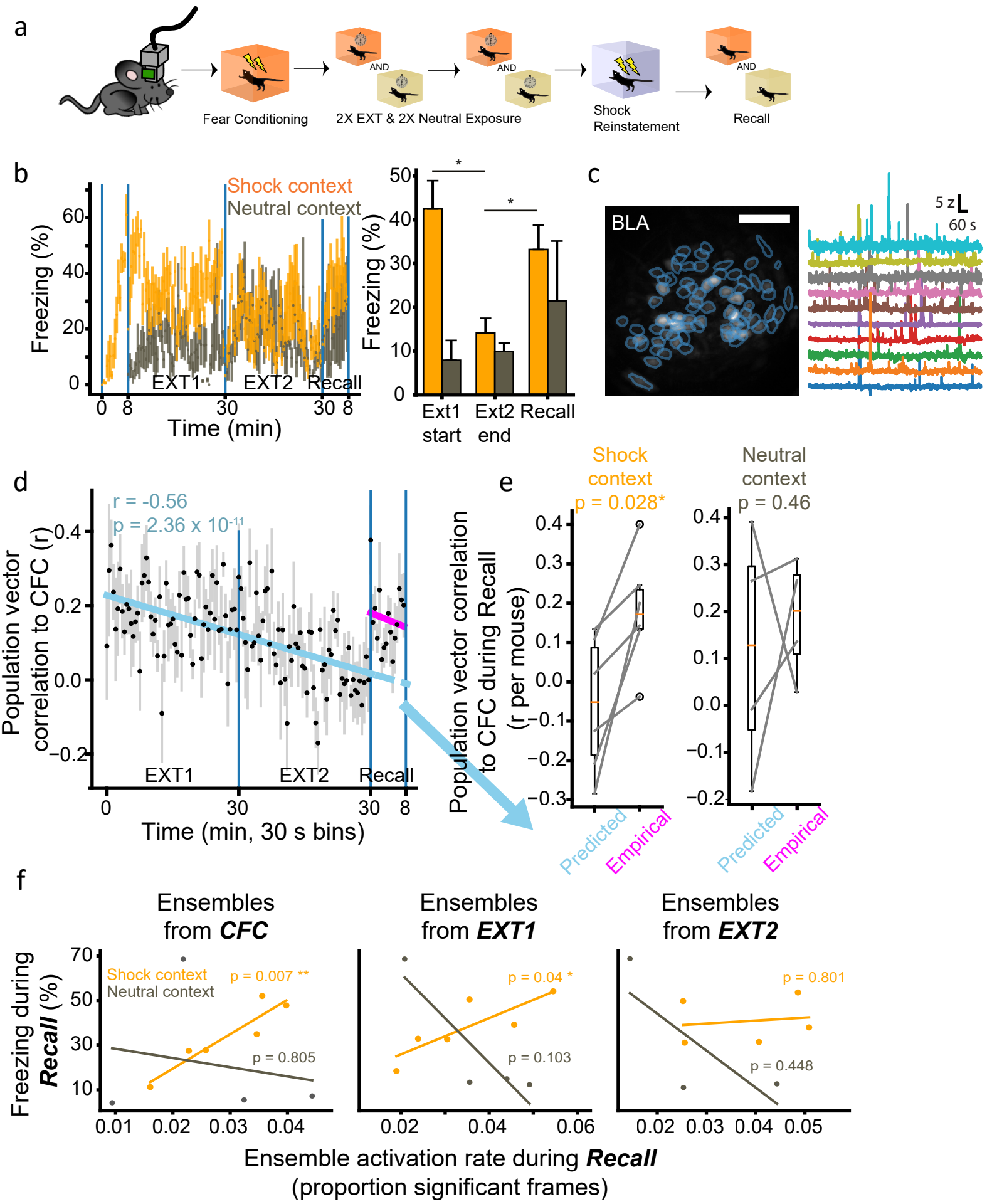
a
Fear Conditioning
AND
2X EXT & 2X Neutral Exposure
AND
Shock Reinstatement
AND
Recall
b
Shock context
Neutral context
Freezing (%)
EXT1
EXT2
Recall
Time (min)
Ext1 start
Ext2 end
c
BLA
5 z
60 s
d
r = -0.56
p = 2.36 x 10-11
Population vector correlation to CFC (r)
EXT1
EXT2
Recall
Time (min, 30 s bins)
e
Shock context
p = 0.028*
Neutral context
p = 0.46
Population vector correlation to CFC during Recall (r per mouse)
Predicted
Empirical
f
Ensembles from CFC
Ensembles from EXT1
Ensembles from EXT2
Freezing during Recall (%)
Shock context
Neutral context
p = 0.007 **
p = 0.805
p = 0.04 *
p = 0.103
p = 0.801
p = 0.448
Ensemble activation rate during Recall
(proportion significant frames)

Figure 2 - figure supplement 1

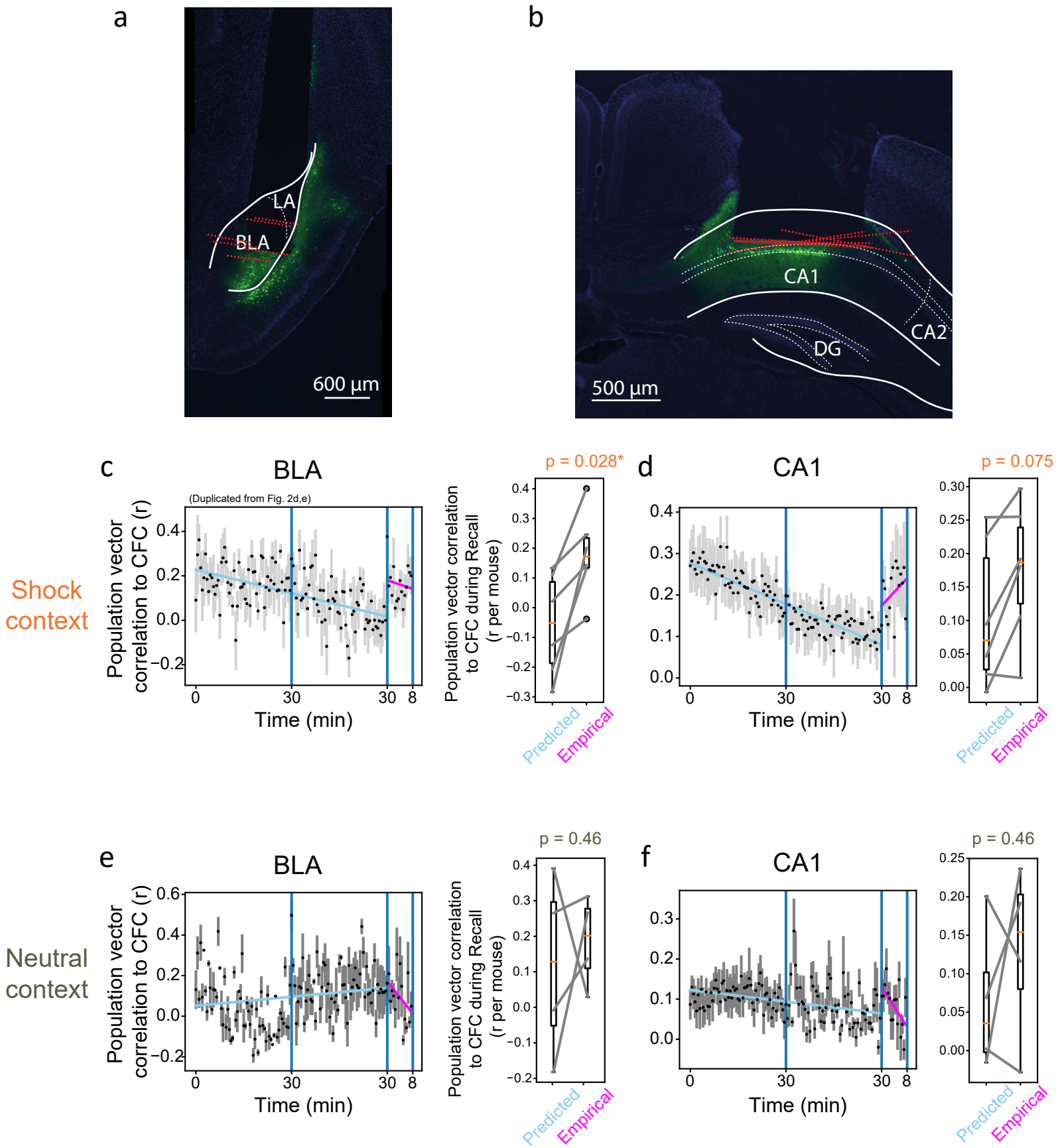

Figure 2 - figure supplement 2

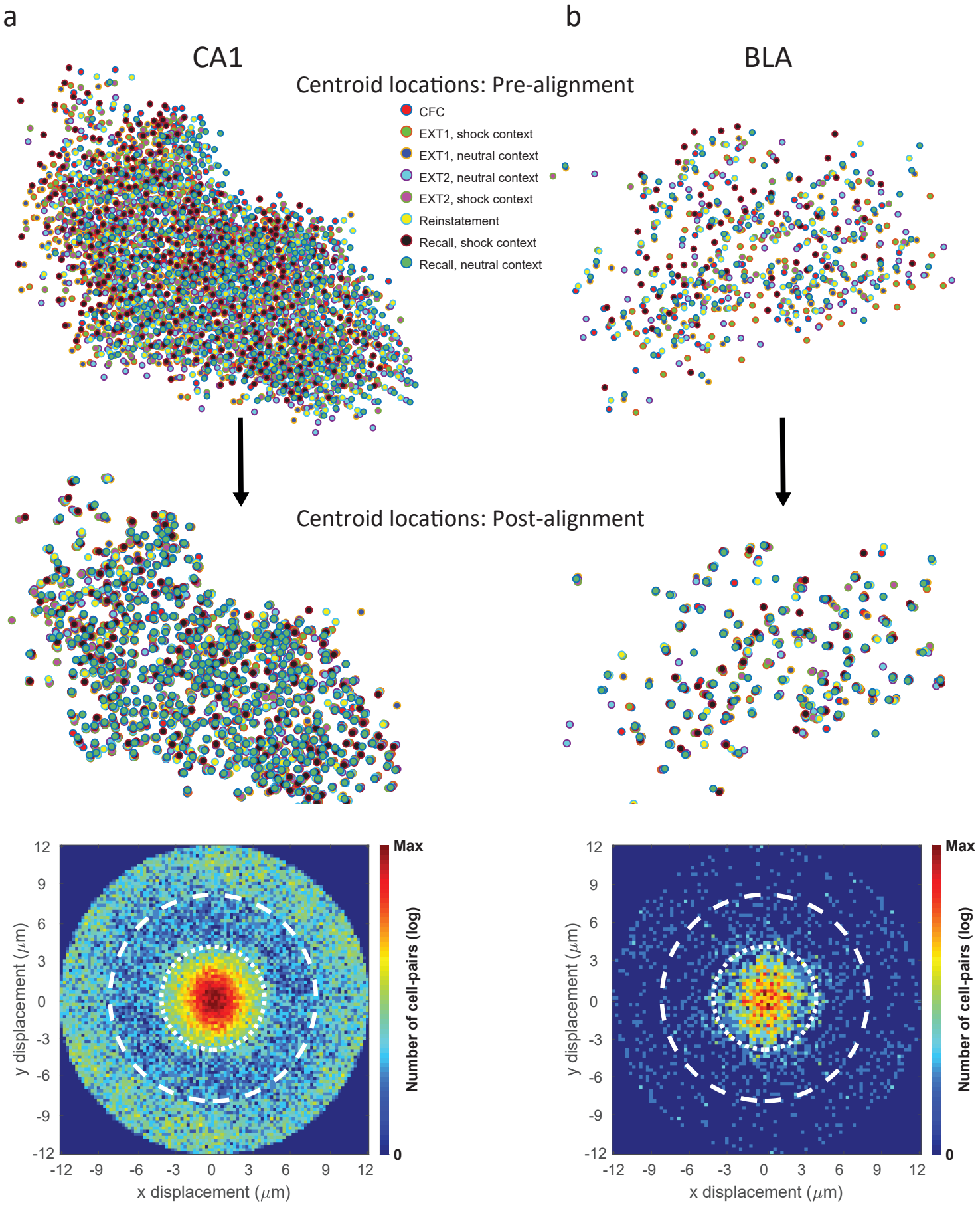

Figure 3

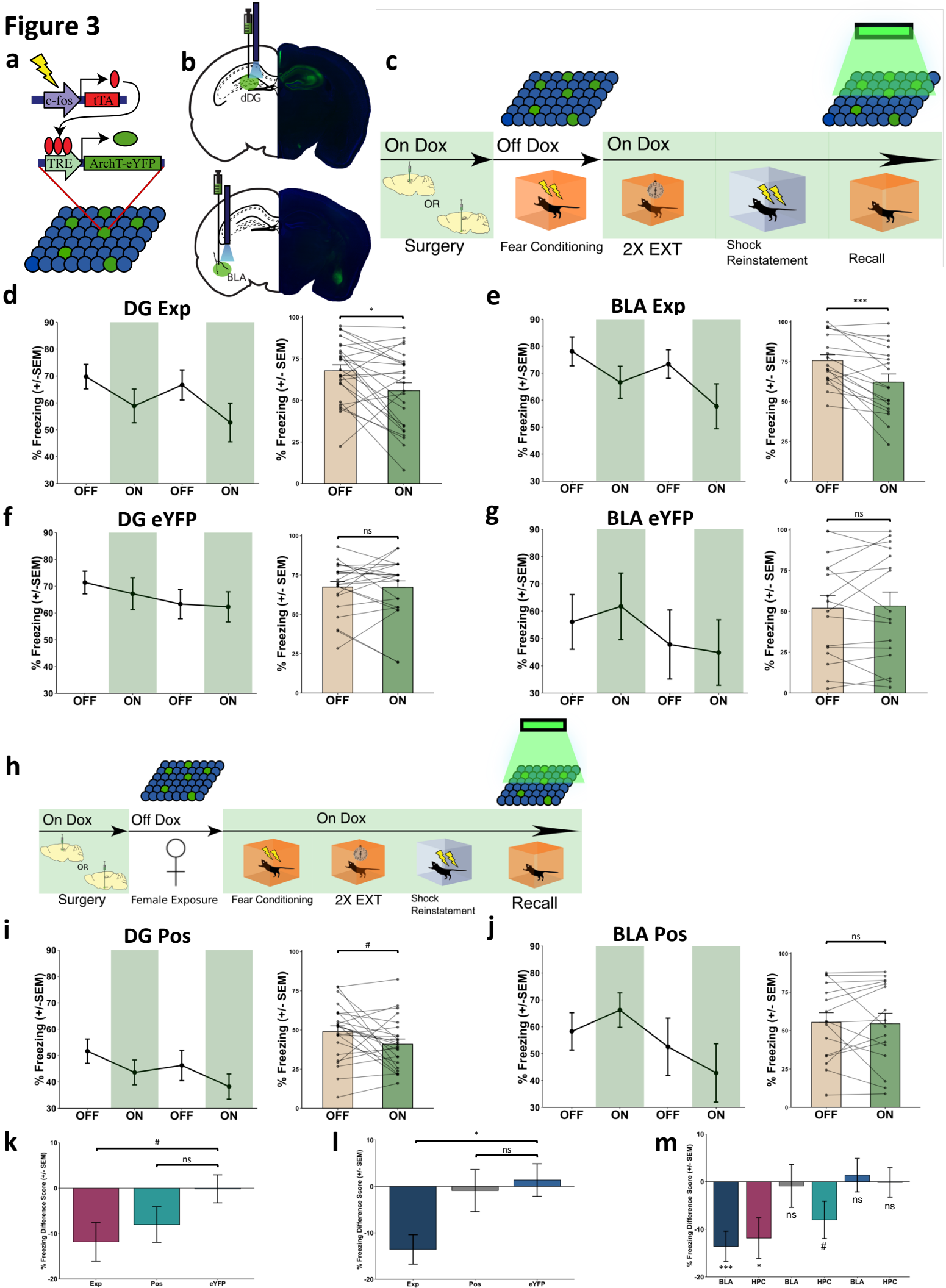
a
c-fos
tTA
TRE
ArchT-eYFP
b
dDG
BLA
c
On Dox
Off Dox
On Dox
OR
Surgery
Fear Conditioning
2X EXT
Shock Reinstatement
Recall
d
DG Exp
% Freezing (+/-SEM)
% Freezing (+/- SEM)
OFF
ON
e
BLA Exp
f
DG eYFP
g
BLA eYFP
h
On Dox
Off Dox
On Dox
Surgery
Female Exposure
Fear Conditioning
2X EXT
Shock Reinstatement
Recall
i
DG Pos
j
BLA Pos
k
% Freezing Difference Score (+/- SEM)
Exp
Pos
eYFP
l
m
BLA
HPC

Figure 3 – figure supplement 1

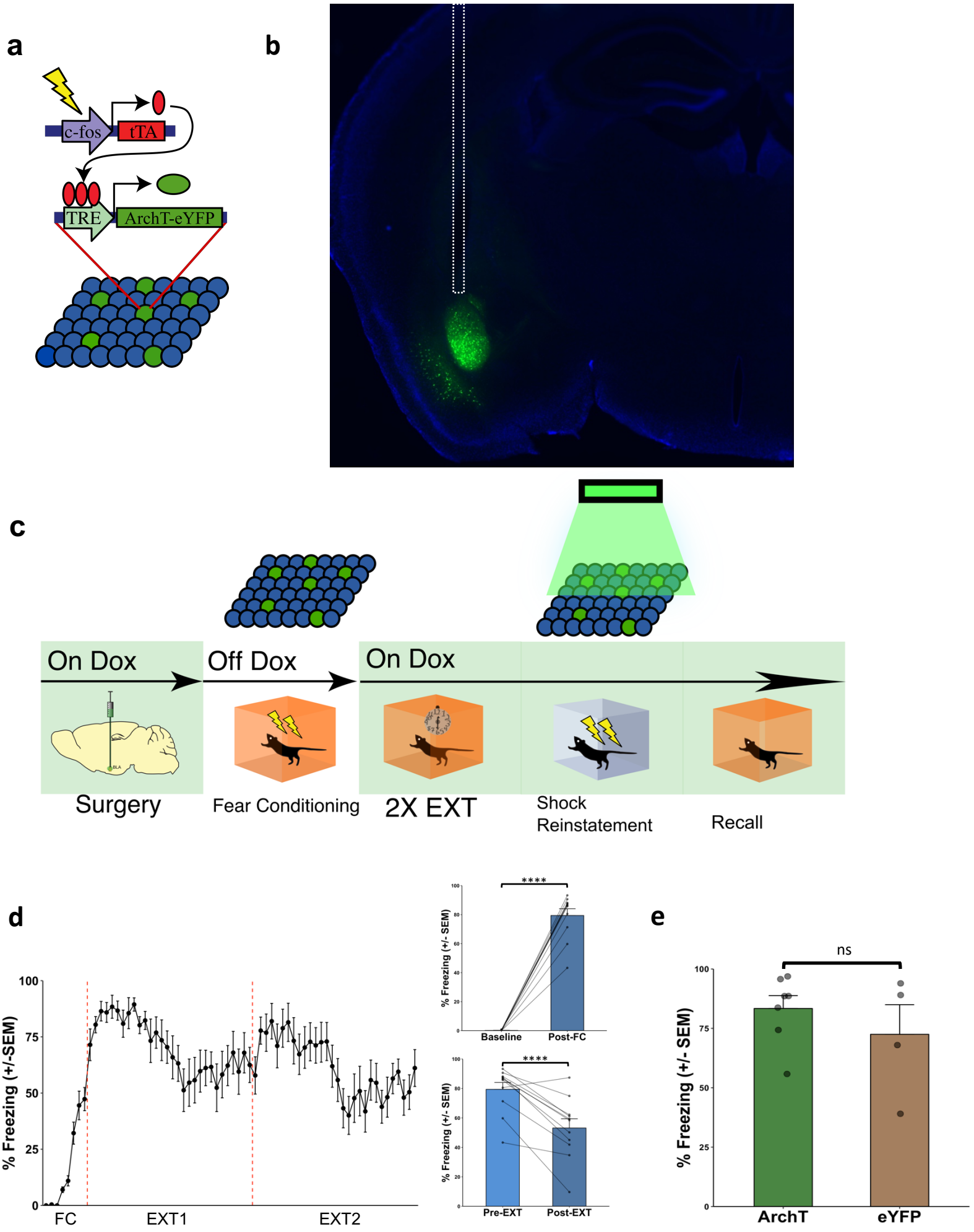

Figure 3 – figure supplement 2

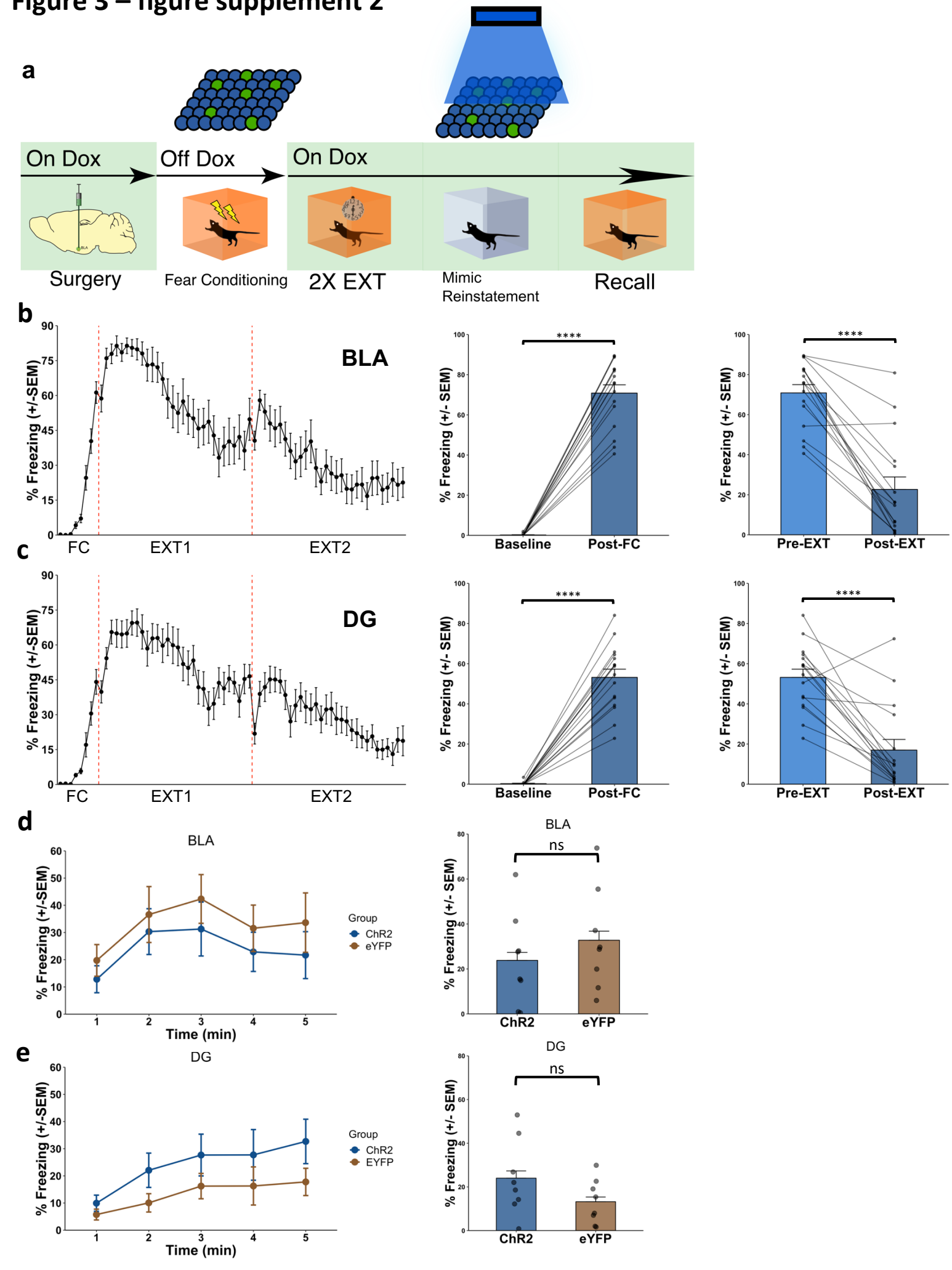
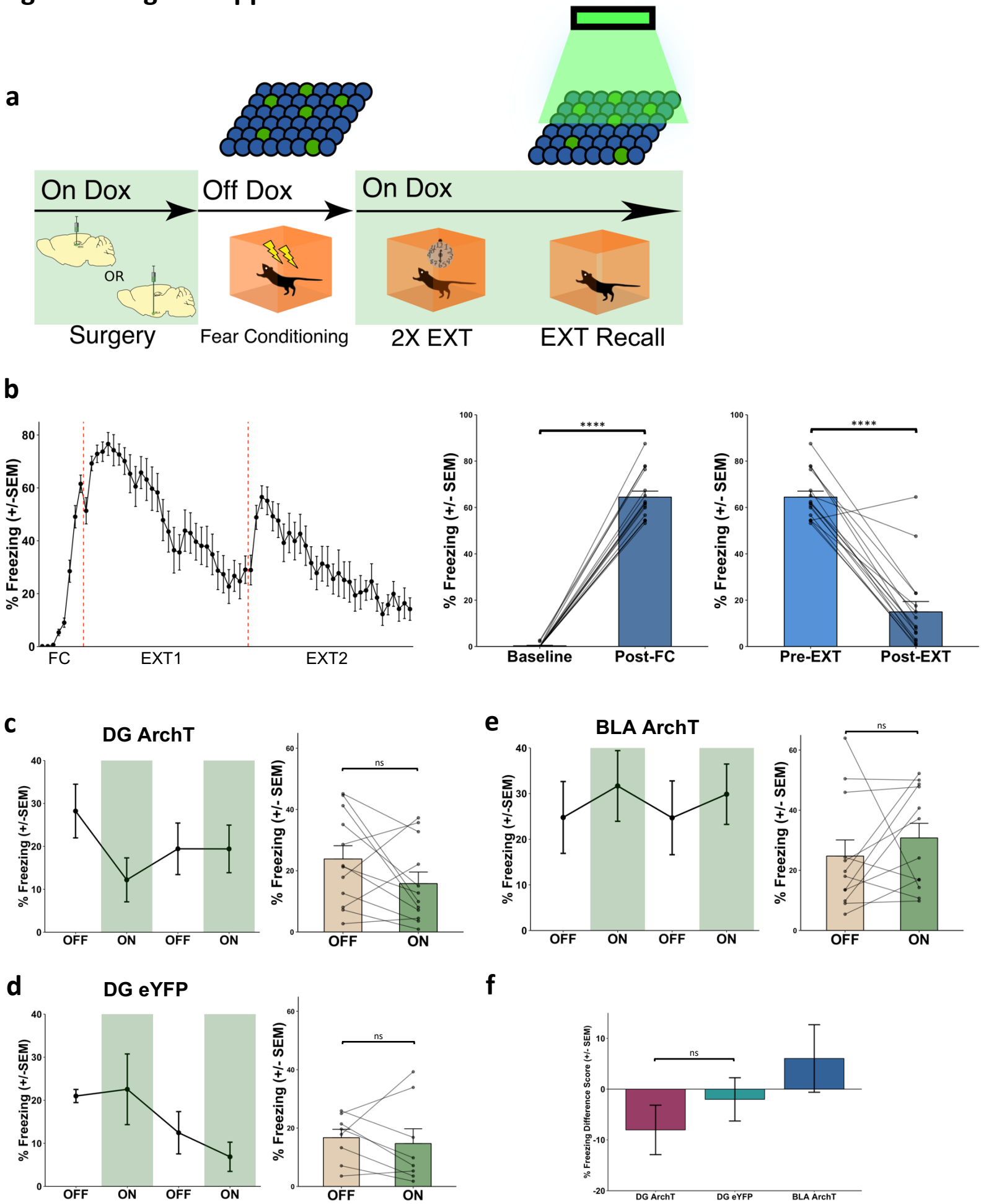
Figure 3 – figure supplement 3